Creep properties of welded joints in OFHC copper for nuclear waste containment

Bo Ivarsson, Jan-Olof Österberg

Swedish Institute for Metals Research

August 1988

CREEP PROPERTIES OF WELDED JOINTS IN OFHC COPPER FOR NUCLEAR WASTE CONTAINMENT

Bo Ivarsson, Jan-Olof Österberg

Swedish Institute for Metals Research

August 1988

IM-2384

CREEP PROPERTIES OF WELDED JOINTS IN OFHC COPPER FOR NUCLEAR WASTE CONTAINMENT

B Ivarsson and J O Österberg
Swedish Institute for Metals Research
Drottning Kristinas väg 48
S-114 28 STOCKHOLM

Keywords: Copper, creep, welded joints, equations, computation

ABSTRACT

In Sweden it has been suggested that copper canisters are used for containment of spent nuclear fuel. These canisters will be subjected to temperatures up to 100°C and external pressures up to 15 MPa. Since the material is pure (OFHC) copper, creep properties must be considered when the canisters are dimensioned. The canisters are sealed by electron beam welding which will affect the creep properties.

Literature data for copper - especially welded joints - at the temperatures of interest is very scarce. Therefore uniaxial creep tests of parent metal, weld metal, and simulated HAZ structures have been performed at 110°C. These tests revealed considerable differences in creep deformation and rupture strength. The weld metal showed creep rates and rupture times ten times higher and ten times shorter, respectively, than those of the parent metal. The simulated HAZ was equally stronger than the parent metal. These differences were to some extent verified by results from creep tests of cross-weld specimens which, however, showed even shorter rupture times.

Constitutive equations were derived from the uniaxial test results. To check the applicability of these equa-

tions to multiaxial conditions, a few internal pressure creep tests of butt-welded tubes were performed. Attempts were made to simulate their creep behaviour by finite differences computer calculations in which the constitutive equations were used. These calculations failed due to too great differences in creep deformation behaviour across the welded joint.

Pages	22
References:	11
Tables:	4
Figures:	20
Appendices:	2

CONTENTS

1 INTRODUCTION

The Swedish Nuclear Fuel and Waste Management Co has suggested a method for nuclear waste disposal where the spent fuel elements after cooling for 40 years in storage pools are placed in prefabricated canisters. The remaining voids are filled with molted lead, after which a tight-fitting lid is electron beam welded on. The canisters are prefabricated to external dimensions of 0.8 m in diameter and 4.5 m in length with a wall thickness of 100 mm.

The encapsulated fuel is intended to be finally disposed of by deposition in a repository at a depth of about 500 m in a selected granitic rock formation. The fuel canisters are deposited in individual vertical holes drilled in storage tunnels. In these deposition holes, the canisters are surrounded by a buffer material consisting of bentonite clay.

The spent nuclear fuel elements will still after 40 years of cooling in the storage pools generate heat and thereby subject the canisters to a temperature of 75-100°C. The surrounding bentonite will in time expand due to ground water absorbtion and as a result expose the canisters to an external pressure successively increasing up to 15 MPa.

This combination of temperature and external pressure is sufficient to cause creep deformation of the canisters, which will eventually change their shape to a slightly hour-glass shaped form. At first, the deformation resistance is low due to the inevitable casting porosity (2%) in the lead surrounding the fuel elements. But when the pores have sintered further deformation will result in a compression of the lead. Thereby a back stress counterbalancing the external pressure is built up in the lead without much further deformation. The canisters are thus

off-loaded and their deformation ceases. It is however of vital importance that the material can withstand the local strains that occur during the 2% inner volume reduction. This aspect must be considered extra carefully for weldments, for which creep ductility and also corrosion resistance normally are lower than for the parent metal.

Thus the creep deformation behaviour and rupture strength of OFHC copper and various parts of weldments therein must be known for the final dimensioning of the canisters. Since no data for weldments and very little data for OFHC parent metal were found in the literature for the temperature range of interest, the present project "Investigation of creep properties in pure copper and weldments in pure copper" was initiated. The main purpose of the project was to determine creep data and to express them in equations readable to computer programs suitable for dimensioning calculations.

Qualitative calculations of the creep deformation in canisters have been performed with the FEM program ADINA at ABB-ATOM (1). The aim of that analysis was to see if the program was suitable for a more accurate analysis. Therefore some simplifications were made: a constant external pressure, a somewhat simplified canister geometry, homogeneous material properties, i.e. no weld present, and a constant creep rate through the whole creep process. This simplified qualitative analysis showed that this program can be used for more accurate calculations if more realistic creep data and geometries are used.

The analysis also indicated that the highest stresses arise where the welded joint between the lid and the canister was suggested to be located.

2 EXPERIMENTAL

2.1 Material and welding procedure

2.1.1 Material

The material used in this project was OFHC copper, delivered from Outokumpu in the form of square forged bars, 100 x 100 mm.

2.1.2 Welding

The welding of the copper was performed at the Welding Institute, Cambridge, England, and is described in detail in Ref. 2. The Welding Institute possesses the experience and equipment for electron beam welding of heavy copper sections. The technique enables joints to be made through a wall thickness of 100 mm in one pass. The resulting joint is very narrow and it is difficult to distinguish the weldment from the parent metal metallurgically.

The testing programme of this project included uniaxial creep testing of all relevant structures in a welded joint. But for an ordinary electron beam weldment the narrowness of the joint makes it impossible to extract the creep test specimens needed for each structure. Therefore, welding was performed with a dispersed electron beam for the manufacturing of cross-weld creep specimens and internal pressure test tubes (see section 2.2.2). For the all weld test specimens a multi-pass weld was necessary. This procedure resulted in a wider weld metal zone from which specimens were extracted longitudinally.

A metallurgical examination reported in Ref. 2 revealed that the grains in the weld fusion zone had less angular boundarier and fewer - if any - twins than the grains in the forged parent metal. In the multi-pass welds there was evidence of recrystallization and twinning grain refinement caused by reheating by subsequent weld passes.

Another evidence of that was a sub-grain structure not found in the single pass weld.

The HAZ structure was similar in both weld types - a coarser structure than in the parent metal as a result of grain growth and/or recrystallization during welding.

Micro Vickers hardness measurements across the welds showed little difference, possibly a slightly higher hardness in the weld metal (90-100) compared with the HAZ and parent metal (80-95).

2.1.3 HAZ simulation

The wider welded joint obtained with the method described in the previous section only enabled specimens to be extracted from the all-weld metal, but not from the HAZ zone. Therefore the HAZ structure was simulated by furnace heat treatment of the parent metal. Several different time - temperature combinations were tested in order to obtain a structure resembling the real HAZ structure. The best combination was found to be 800°C, 1h, air cooling.

2.2 Testing procedure

2.2.1 Uniaxial tests

Specimens with 5 mm diameter and 50 mm gauge length were used in all uniaxial tests. Four different structure types were tested: parent metal, weld metal, simulated HAZ, and cross-weld specimens. All types were tested at 110°C, but the parent metal was additionally tested at two other temperatures, 75 and 145°C.

The uniaxial testing was carried out at the Swedish Institute for Metals Research in single specimen constant load creep testing machines. The elongation was measured at intervals ranging from several times per hour down to

once a week depending on the stress, tested structure, and present stage of creep.

All specimens except a few (which were discontinued) were run until rupture. One test (parent metal, 75°C, 100 MPa) is still running and has probably not reached the minimum creep rate.

Since the cross-weld specimens were cut out with the gauge length perpendicular to and across the single-pass welded joint they consisted of several structures. The elongations were followed separately for each structure. Therefore the cross-weld specimens were off-loaded intermittently and removed from the machine for measurement of the elongation in each structure. To accurately distinguish the diffuse boundaries between the structures for precise measuring of their respective elongation, small Vickers microhardness indentations were made at each boundary.

2.2.2 Internal pressure tests

Besides the above-mentioned uniaxial tests, four tests of tubular specimens with circumferential welds under internal pressure were performed. The reason for this is twofold - it is of great interest to determine the multiaxial creep behaviour of welded joints. Moreover, the results were to be used to check the accuracy of computer simulations of the behaviour, in which constitutive equations derived from the uniaxial creep tests are used. The specimens were 100 mm long and had an outer diameter of 20 mm. Two specimens had a wall thickness of 2.85 mm while the walls of the other two were 0.9 mm thick. The specimens were not manufactured by butt welding two tubes, since the low heat input required to join thin-walled tubes would give weld and HAZ structures notably different from that expected in the canisters. Instead, specimens blanks were cut perpendicular to the single-pass welded joint from which uniaxial cross-weld speci-

mens were taken. These blanks were then bored and turned to the above-mentioned dimensions. The welds were situated at the middle of the tube length.

The internal pressure tests were carried out at AB Sandvik Steel in Sandviken. Filler rods allowing longitudinal expansion and contraction were inserted in the tubes, which were then sealed (by brazing), heated to 110°C in a furnace, and pressurized with argon. The pressure levels were chosen to give hoop stresses ranging from 80 to 120 MPa. The tests were interrupted intermittently for strain measurements. The strain was measured as increase in diameter at 14 locations along the tube. Rupture was indicated by loss of argon pressure through small leaks.

3 CREEP TEST RESULTS

3.1 Uniaxial tests

The test results are presented in Table 1. Results for all 110°C tests are plotted in Figs. 1-3 as stress vs. rupture time, stress vs minimum creep rate, and ductility (elongation and area reduction) vs. rupture time, respectively. Figs. 4-6 are the corresponding figures for parent material at 75, 110, and 145°C.

The straight lines in Figs. 2 and 5 represent the Norton equation

$$\dot{\varepsilon} = B \cdot \sigma^m. \qquad (1)$$

B and m values are given in Table 1.

In Fig. 1 the creep rupture strength decreases in the order simulated HAZ, parent metal, weld metal, and finally [and weakest] the cross-weld.

In comparison to the parent metal results the simulated

HAZ structure exhibits considerably longer rupture times while the weld metal rupture times on the other hand are about a factor ten shorter.
Fig. 2 shows the same ranking between the three structures when creep deformation strength is considered. The difference between parent and weld metal is, however, somewhat smaller.

The results in Fig. 4 show that a 35 degrees increase in temperature leads to an decrease in rupture time with a factor 20 or more - a factor increasing with decreasing stress.

Fig.5 shows the same temperature dependence for the minimum creep rate. In fact the creep rate difference between 75 and 110°C increases very rapidly with decreasing stress.
In Fig. 7 the time variation of strain in the various zones and the average strain of the highest stress cross-weld specimen is exemplified. It is obvious that the deformation is greatest in the weld metal. In fact rupture occurs before the parent metal and the HAZ have reached the minimum creep rate. Hence, the minimum creep rate can only be evaluated for the weld metal and is included in Fig. 2.

For cross-weld tests at lower stresses the deformation is even more concentrated to the weld metal. This fact resulted in too sparse strain measurement off-loadings so that accurate minimum creep rates could not be evaluated. Since all cross-weld specimens ruptured in the weld metal their rupture times which are included in Fig. 1 should be compared with those of the homogeneous weld metal. The cross-weld rupture times are obviously shorter; the difference increasing rapidly with decreasing stress.

Another detail in Fig. 7 that must be commented is the fact that the HAZ part of the specimen show a higher strain than the parent metal, contrary to what one would

expect judging from Fig. 2.
In Fig. 8 the 120 MPa, single structure creep curves for parent and weld metals and simulated HAZ structure are plotted in the same scale as in Fig. 7 to facilitate the comparison. The HAZ creep deformation is very low while the parent and weld metals shows approximately equal primary creep deformation. In fact, at lower stresses primary creep is faster in the parent metal than in the weld metal. But on the other hand, onset of tertiary creep occurs much earlier in the weld metal thus causing the considerably higher minimum creep rates shown in Table 1 and Fig. 2.

3.2 Internal pressure tests

Three of the four tested tubes have ruptured and the fourth test is in progress. All specimens ruptured in the weld metal with no specific preferential orientation.

Detailed information on the tested tubes is given in Table 2. The rupture times are plotted in Fig. 1 against the maximum stress, i.e. the hoop stress.
In Figs. 9-12 the measured diametral strain distributions at different times during testing and at rupture are plotted. For all specimens rupture occurred in the welded joint, close to the fusion boundary.
Figs. 10 and 11 indicate that for specimens 300-1 and 4 secondary creep rates (between 132 and 500h and between 100 and 267h, respectively) can be determined at least for parent and weld metal. These values are included in Fig. 2, plotted against the effective stress (~0.87 times the hoop stress) which usually controls the deformation behaviour.

4 ANALYSIS OF UNIAXIAL DEFORMATION BEHAVIOUR

4.1 Creep properties

Besides the time and creep strain values recorded in all tests, creep rate data were required for the determination of constitutive equations. For that reason, strain was plotted against time for each test and curves were manually faired to the data points. Creep rates were then evaluated as tangents to those curves at various strains and times.

In previous studies of the creep behaviour of welded joints in steel, the creep deformation and rupture behaviour of internal pressure tested butt-welded tubes has successfully been simulated (3-7). Therefore, the same type of constitutive equations have been used in the present analysis. They are described in detail in Appendices A and B of Ref. (7), which are also included in this report.

The computer program used was originally developed for secondary creep only, thus requiring the constants B and m in the Norton equation, Equation (1).

To account for primary or tertiary creep, strain dependent constants were introduced - the most suitable expression was:

$$\dot{\varepsilon} = 10^{(c+e\cdot\log\varepsilon)} \cdot \sigma^{(d+f\cdot\log\varepsilon)} \qquad (2)$$

i.e. equation (B4) in Appendix B where e is negative for primary creep and positive for tertiary creep. Moreover, in this investigation it was found that f could be set equal to zero. c, e, and d values were determined with regression analysis. These values which were used in the computer calculations are listed in Table 3. The transition from primary to tertiary creep was found by equating

the corresponding equations. This transition occurred at a time dependent strain level.

In Fig. 13 experimental creep curves for parent metal tested at 110°C are compared with curves calculated for the values in Table 3.

In this Table c, e, and d values for parent metal at three temperatures are given, but since these constants were evaluated independently, there are no simple equations for rationalizing the temperature dependence. Of course a suitable temperature dependent expression could be postulated and a reanalysis for all parent data could be performed - obviously with less good fit. This has however not been done since this type of equation cannot easily be used in ADINA calculations anyway.

In ADINA (8) creep deformation is expressed with one of the following equations:

$$\varepsilon = a_0 \cdot \sigma^{a_1} \cdot t^{a_2} \tag{3}$$

$$\varepsilon = b_0 \cdot e^{b_1 \cdot \sigma} \cdot (1 - e^{-b_2 \cdot (\frac{\sigma}{b_3})^{b_4}}) + b_5 \cdot e^{b_6 \cdot \sigma} \cdot t \tag{4}$$

$$\varepsilon = c_0 \cdot \sigma^{c_1} \cdot (c_2 \cdot t + c_3 \cdot t^{c_4} + c_5 \cdot t^{c_6}) \cdot e^{-\frac{c_7}{T+273.16}} \tag{5}$$

The first two equations are isothermal and describe primary and primary + secondary creep, respectively. In Equation (4), one of the constants b_2 and b_3 is redundant and can be set equal to unity.
The same goes for c_o and c_2 in Equation (5). This equation consists of three parts describing stress, time, and temperature dependence. The time dependent part can be used for entire creep curves provided $0 < c_4 < 1$ and $c_6 > 1$ or vice versa. This separable time function makes Equation (5) impossible to use for the present data where rupture times vary over several orders of magnitude.

The constants in Equations (3) and (4) have been evaluated with least square methods and are presented in Table 4. The corresponding creep curves are compared to experimental curves for parent metal at 110°C in Fig. 14, c.f. Fig. 13.

4.2 Tensile properties

In the computer program used for simulation of the creep behaviour of the internal pressure tested tubes, only elastic and creep deformation can be calculated. Thus the plastic deformation on pressurization has to be estimated separately.

The plastic deformation on loading has been determined for the uniaxial creep test specimens. The results were fitted to the following expression (4)

$$\varepsilon_{pl} = (\sigma/\sigma_*)^n. \qquad (6)$$

At 110°C the values for σ_* (MPa)/n were 235/4.9, 185/8.1, and 520/3.8 for parent metal, weld metal, and simulated HAZ, respectively.

Following Ref. (4), the plastic strains on pressurization can be evaluated as

$$\epsilon_\theta = (0.75)^{\frac{m+1}{2}} \cdot (\sigma_\theta/\sigma_*)^m \qquad (7)$$

The calculated values are included in Table 2.

5 COMPUTER CALCULATIONS

A finite difference computer program was used for the calculations (9). The program was initially developed for calculation of creep deformation and buckling of axisymmetric shells. However, previous experience (3-7) has shown that it as a rule is excellent for calculations of creep deformation under internal pressure. Only in one case (7) no convergent solutions were achieved - an effect of a too great difference in creep rate at a fusion boundary.

Unfortunately this was also the case in the present calculations where the creep deformation strength of the HAZ was much higher than the parent and weld metal strength. A few calculations were therefore performed with no HAZ and with a somewhat (a factor ten) weaker HAZ. The results of these calculations are presented in Figs. 15-18, where Fig. XXa shows results from calculations with no HAZ and Fig. XXb shows the modified HAZ results. All results presented were calculated for specimen number 4.

Figs. 15a and b show the hoop stress profiles for one half of the symmetric welded tube at various times. On the x-axis in these figures, symbols are plotted at various locations. The time variation of hoop stress at these positions is given in Figs. 16a and b where these symbols are used. Figs. 17 and 18 show the corresponding results for diametral strain and should be compared to the experimental results in Figs. 9-12. The other calculated stresses and strains are of less importance. The axial strain is almost constant in time and space and is equal to 0.5 times the original hoop stress. The axial strain is about an order of magnitude smaller than the tangential strain. Bending moments and strains were negligibly small as were the transverse forces.

The stress redistributions illustrated in Figs. 16a and b lead to an equalization of the creep rates in different parts of the tubes. Besides the initial changes there is another considerable change starting after 1000h in Fig. 16a and 2000h in Fig. 16b indicating the transition from primary to tertiary creep in the weld metal. From Figs. 16a and b the location of and time to rupture can be estimated by summing the creep damage at different positions over small time intervals. In both cases rupture was predicted to occur in the weld metal after 950 and 2500 hours respectively.

Fig. 17 shows that except for the end effects the strain is almost uniform across the HAZ-free tube until the onset of weld metal tertiary creep, when this part starts bulging. In the modified HAZ calculations, deformation in the weld region is restrained by the HAZ but a bulging is predicted when the tertiary creep stage is reached in the weld metal.

6 DISCUSSION

6.1 Welding procedure

One must bear in mind that the welding procedure applied in this investigation deviates considerably from normal procedure. Although the water cooling during welding was efficient, the higher heat input required to produce the wider welds and the multi-pass welding is likely to have resulted in HAZ and weld metal creep properties different from those of a normal weld. The magnitude of these differences is difficult to estimate, but judging from the pronounced microstructural differences it may be considerable.

6.2 Uniaxial creep tests

The uniaxial creep strength difference between the three structures tested is not unexpected. At least for various steels the cast weld structure shows a lower creep strength than the parent metal but as a rule equal or higher ductility. The hardened HAZ structure, on the other hand, has a higher strength but often lower ductility.
Fig. 3 shows that the area reduction values for the weld metal and the simulated HAZ are equal to those of the parent metal. The elongation values are however somewhat smaller. In spite of that, the ductility is high enough to allow stress redistribution during multiaxial loading.

The values for the Norton exponent given in Table 1 are rather high in comparison with the ordinary values for dislocation creep (3-5) - especially for parent metal at 75°C. The reason for this deviation can be found in Ref. 10. The stress levels used in this investigation fall in the region where transition from (low stress) power law creep to the so called power law breakdown occurs, see Fig. 19. This must be taken into account when data are extrapolated to lower stresses.

In Fig. 6 the 75 and 110°C tests show approximately the same ductility. For the 145°C both the elongation and area reduction values are lower with possibly a minimum around 1000 hours. But since the canisters are not expected to reach such high temperatures this low ductility is less important. However, Fig. 20 which is reproduced from Ref. 11 shows that this minimum is connected with the transition from transgranular to intergranular failure. Therefore, a ductility minimum is also expected at lower temperatures/lower stresses/longer times. This must be studied further.

The behaviour of the cross-weld specimens is somewhat puzzling. In the single structure tests the parent metal primary creep rate was approximately equal to that of the weld metal and much faster than that of the simulated HAZ cf Fig. 8. But in almost all cross-weld specimens the parent metal parts show the smallest creep deformation. The reason for this behaviour is probably a combination of a considerably weaker weld metal and the fact that the HAZ part of the specimens contains some weld metal.

All ruptures occurred in the weld metal part with much shorter rupture times than in the all weld specimens. This reduction in life can be given several explanations:

* different weld methods were used for the two specimen types. Possibly the recrystallization during multi-pass welding can have resulted in a more creep resistant structure.

* the localization of creep deformation to the small weld metal part of the specimens will lead to stress concentrations and accelerated creep.

* the creep strength may be lower in the transversal than in the longitudinal direction. This is serious since

the calculations in Ref. 1 show that the highest stresses on the welded joint will be in the transversal direction.

6.3 Internal pressure tests

The use of two wall thicknesses in the tested tubes is not deliberate but a result of a misunderstanding and the tubes being manufactured at two occasions. It is impossible to determine from the present results if the difference in thickness has had any influence on the deformation and rupture behaviour.

The uniaxially tested cross-weld specimens all ruptured in the weakest zone - the weld material. But in multiaxial tests (or in uniaxial tests where the different zones are loaded in parallel, not in series) rupture does not necessarily occur in the zone with the lowest creep strength. For the previously studied steels rupture was often predicted to occur in the strongest zone - the HAZ. Due to its high deformation resistance, stress peaks were built up in that area and caused rupture as a result of insufficient rupture strength and/or ductility.

In the present investigation all tubes ruptured in the weld metal implying that the differences in strength were too large to be overcome by the stress redistribution. In fact, the rupture times coincide with those of the cross-weld specimens, c.f. Fig. 1. The creep rates for parent and weld metal included in Fig. 2 are considerably higher than for the corresponding uniaxial tests, and would be so - at least for the parent metal - even if plotted against maximum stress. To some extent this is caused by the initial plastic deformation on pressurization which results in an increase in diameter and a decrease in wall thickness and thereby in stresses higher than the nominal ones. Moreover it is likely that the evaluated parent

metal creep rates are not minimum values, c.f. Fig. 13. The difference between internal pressure weld metal and all weld specimen creep rates is in agreement with the difference in rupture time and reflects the above-mentioned difference between single- and multi-pass weldments.

The asymmetric strain distribution - especially in Fig. 11 - is established already on pressurization. During the initial creep stages creep rates are fairly constant - perhaps somewhat higher in the more deformed parts where creep acceleration also is more pronounced.

6.4 Creep curve analysis

One major difference between the present copper creep curves and those analysed previously (3-7) for different steel types is that in the present curves the primary creep stage is much more pronounced, c.f. Fig. 13. Actually, in many cases the tertiary stage, if present, was too short to be recorded properly.

The fact that most tests were carried out in the boundary between power law creep and power law break-down made it difficult to get a perfect fit to the equations in section 4.1. Fig. 13 shows that Equation (2) gives a satisfactory agreement between experimental and calculated curves. The ADINA equations ((3)-(5)), if applicable at all, give a poorer fit - especially at longer times, see Fig. 14. But for the calculations the primary creep stage is of greatest interest. In this region Equation (3) gives the best fit to experimental data, and should thus be preferred.

6.5 Computer calculations

Since no solutions were obtained with actual HAZ creep data, the solutions for no and for a weak HAZ must be analyzed and extrapolated to actual behaviour.

The stress redistribution behaviour most clearly shown in Figs. 15a and b would be even more pronounced for actual data. The weld metal would be even more off-loaded which would lead to a more delayed onset of tertiary creep and rupture. The HAZ stress peak would be higher, possibly shifting rupture location to that area. Fig. 17 indicates that this stress redistribution would lead to even less creep deformation in the weld/HAZ part.

Comparisons with experimental results, Figs. 9-12, show this to be true in one case - Fig.12. But in Figs. 9 and 10 there is a weld metal bulge already in the first measurements. This is probably caused by an earlier onset of tertiary creep - a result of more plastic deformation on loading than predicted, c.f. section 4.2 and Table 2. In fact, one specimen (400-1, similar to specimen 400-2) ruptured (leaked) on pressurization. For this specimen diametral strain between 4.5% (parent metal) and 3.4% (weld metal/HAZ) were measured, c.f. 1.4 and 0.2% respectively in Table 2.

This extensive plastic deformation can to some extent explain the short rupture times. Another possible explanation is the same as for the difference between all weld and cross-weld specimens, i.e. specimen orientation or weld procedure.

7 CONCLUSIONS

This investigation has shown that there exist considerable differences in creep deformation and rupture strength between different zones in an electron beam welded joint in OFHC copper, the weld metal being weakest and the HAZ being strongest. This effect can to some extent be the result of a non-normal welding procedure.

The above mentioned differences resulted in a concentration of the deformation in cross-weld specimen to the weld metal. In internal pressure tested tubes stress redistribution resulted in an equal or even greater deformation in the parent metal. The HAZ showed the smallest deformation but was subjected to the highest stresses, according to calculations.

Since the creep testing was performed at, or slightly above, the expected service temperature the stress levels had to be rather high in order to get reasonable rupture times. Unfortunately the stress ranges used were on the boundary between power law creep and power law breakdown. Therefore, extrapolations to the expected service stress levels are somewhat uncertain.

The uniaxial creep ductility was in almost all cases sufficiently high to allow stress redistributing deformations under multiaxial loads. For parent material at the highest temperature and hence lowest stress a ductility minimum was found. This indicates that the presence of a low ductility stress/time region cannot be ruled out for lower temperatures.

Weld metal creep behaviour was different in all weld and cross-weld specimens. There are several possible explanations for this behaviour.

One type of constitutive equations, previously used in calculations of creep behaviour of internally pressuriz-

ed, welded steel tubes, gave a satisfactory fit to experimental data. The fit for equations to be used in planned FEM calculations were less satisfactory but acceptable in the primary creep region. Loading strains for uniaxial creep tests were used to estimate the strain on loading in internal pressure creep tested welded tubes. These strains were underestimated.

Finite difference calculations of the creep behaviour of these tubes failed due to too great differences in creep behaviour between HAZ and parent metal. Calculations with no and with a considerably weaker HAZ gave results that could be extrapolated to qualitatively predict the actual behaviour of the tubes.

8 FUTURE WORK

Although this investigation has given many valuable results, some problems have to be studied further.

* to enable extrapolations to low stress levels where power law or even dislocation creep is dominant, a few creep test series has to be performed at higher temperatures. This will also shed some light on the possible presence of ductility minima.

* in order to find the reason for the difference between all weld and cross-weld specimens, attempts will be made to extract all weld specimens from the single pass weldment. Results from creep testing of these specimens would make it possible to decide if the difference is a result of different specimen orientation or different welding procedure.

* the prediction of plastic deformation on loading must be improved.

* a constitutive creep equation, suitable for ADINA calculations and describing entire creep curves accurately should be developed.

* in the present investigation non-normal welding procedures were applied, which probably led to increased differences in tensile and creep properties across the welded joint. Therefore, welds should be manufactured with optimized procedures and creep tested. For the resulting narrow joints only cross-weld and internal (or preferably external) pressure tests are possible.

ACKNOWLEDGEMENTS

This project has been financed by Svensk Kärnbränslehantering AB, SKB, (Swedish Nuclear Fuel and Waste Management Co) which is gratefully acknowledged.

The experimental work was planned by Lars Yngrén and has been performed by Elon von Walden. Thanks are also due to Lars Werme, SKB and Rolf Sandström, SIMR for valuable and stimulating discussions during planning and performance of the project.

REFERENCES

1. LANDSTRÖM, A.,
KBS - Creep Analysis of a Copper Canister using ADINA. Final Report (In Swedish) ASEA ATOM, Internal Report KUA 84-263, (1984).

2. SANDERSSON A. and PUNSHON, C.S.,
EB Weldability Trials and Production of Creep Test Samples in Forged OFHC Copper. Welding Institute Report 23839/1/87, (1987).

3. IVARSSON, B. and SANDSTRÖM, R.,
Creep Deformation and Rupture of Butt-Welded Tubes of Cold Worked AISI 316 Steel. Metals Technology, 7 (1980), 440-448.

4. IVARSSON, B.,
Creep of Butt-Welded AISI 316 (18Cr-13Ni-3Mo Steel) Tubes: Role of Plastic Strain and Primary Creep. Metals Technology, 9 (1982), 41-45.

5. IVARSSON, B.,
Creep Deformation and Fracture in Butt-Welded 12% Chromium Steel Tubes. Swedish Institute for Metals Research, Internal Report IM-1748, (1983).

6. IVARSSON, B.,
Computer Simulation of Creep Deformation in Butt-Welded 1%Cr0.5%Mo Steel Tubes. Swedish Institute for Metals Research, Internal Report IM-1820, (1983).

7. IVARSSON, B.,
Creep Deformation and Rupture in Butt-Welded Alloy 800H Tubes. Swedish Institute for Metals Research, Internal Report IM-1893, (1984).

8. Automatic Dynamic Incremental Nonlinear Analysis, System Theory and Modeling Guide, Report AE 83-4, Adina Eng., Sept. 1983.

9. SAMUELSSON, L.A.,
Creep Buckling of Shells of Revolution. User's Manual for Program DSOR 06. The Aeronautical Research Institute of Sweden, Internal Report, HU - 1543, part 4, (1975).

10. FROST, H.J. and ASHBY, M.F.,
Deformation - Mechanism Maps. The Plasticity and Creep of Metals and Ceramics. Pergamon Press, Oxford, (1982).

11. ASHBY, M.F.,
Fracture Mechanism Maps, Cambridge University Engineering Dept., Report CUED/C/MATS/TR.34, (1977)

Table 1. Uniaxial creep test result

Structure	Temperature (°C)	Stress (MPa)	Rupture time (h)	Minimum creep rate (h^{-1})	Elongation A_c (%)	Reduction in area Z_c (%)	B	m
PM	75	100	28500*)	~$1.8 \cdot 10^{-7}$*)	-	-		
		140	6300	$8.6 \cdot 10^{-6}$	19.5	31.1		
		145	7840	$3.2 \cdot 10^{-6}$	17.7	32.8	$1.14 \cdot 10^{-63}$	26.77
		150	1697	$1.6 \cdot 10^{-5}$	12.5	32.8		
		160	464	$1.1 \cdot 10^{-4}$	28.2	42.0		
		170	110	$8.0 \cdot 10^{-4}$	35.6	45.0		
PM	110	100	7000	$4.8 \cdot 10^{-6}$	10.6	24.5		
		110	5890	$6.7 \cdot 10^{-6}$	9.8	22.6		
		120	1430	$2.0 \cdot 10^{-5}$	15.2	26.6	$1.50 \cdot 10^{-31}$	12.64
		130	661	$5.5 \cdot 10^{-5}$	16.5	36.0		
		140	168	$2.2 \cdot 10^{-4}$	20.8	35.7		
		150	60	$6.7 \cdot 10^{-4}$	15.3	36.0		
PM	145	75	5356	$2.8 \cdot 10^{-6}$	4.9	22.6		
		85	1775	$5.0 \cdot 10^{-6}$	4.4	14.7		
		90	735	$2.3 \cdot 10^{-5}$	6.0	12.0	$6.77 \cdot 10^{-26}$	10.42
		100	650	$4.4 \cdot 10^{-5}$	10.8	26.1		
		110	265	$1.1 \cdot 10^{-4}$	12.5	21.3		
		120	110	$3.5 \cdot 10^{-4}$	15.9	26.9		

*) still running

Table 1. - Cont'd

Structure	Temperature (°C)	Stress (MPa)	Rupture time (h)	Minimum creep rate (h^{-1})	Elongation A_c (%)	Reduction in area Z_c (%)	B	m
WM	110	80	16605	$\sim 2 \cdot 10^{-7}$	2.7	18.7		
		100	2065	$1.1 \cdot 10^{-5}$	5.8	25.1	$1.06 \cdot 10^{-41}$	17.99
		110	456	$3.1 \cdot 10^{-5}$	9.5	39.1		
		120	30	$\sim 4.1 \cdot 10^{-4}$	9.5	41.5		
Sim HAZ	110	120	14523	$2.0 \cdot 10^{-6}$	4.4	28.9	$1.57 \cdot 10^{-44}$	18.31
		135	2105	$1.4 \cdot 10^{-5}$	6.8	26.3		
		150	408	$1.2 \cdot 10^{-4}$	13.7	31.4		
CW	110	60	3866	-	-	-		
		80	510	-	-	-		
		100	445	-	-	-		
		100	223	-	-	-		
		120	36	$\sim 2.2 \cdot 10^{-4}$	-	-		

Table 2 Internal pressure creep tests at 110°C

Specimen number	Outside diameter (mm)	Wall thickness (mm)	Internal pressure (MPa)	Calculated hoop stress (MPa)	Rupture time (h)	Maximum diametral strain %	Calculated plastic hoop strain on loading (%)		
							PM	WM	Sim HAZ
400-2	19.8	2.83	39.2	117.5	35	7.0	1.43	0.68	0.18
4	19.9	0.91	10.3	107.5	285	6.9	0.93	0.33	0.13
300-1	19.9	2.85	29.4	88	697	4.6	0.35	0.07	0.06
5	19.95	0.95	7.85	78.5			0.20	0.03	0.04

Table 3 Equation (2) constants determined in the analysis of uniaxial creep curves

Structure Temperature	Creep stage	c	e	d
PM 75°C	Primary	-41.278	-2.55	15.45
	Tertiary	-20.683	3.0	8.276
PM 110°C	Primary	-46.008	-3.3	17.74
	Tertiary	-21.479	2.5	9.710
PM 145°C	Primary	-40.153	-2.3	16.05
	Tertiary	-5.475	2.3	2.298
WM 110°C	Primary	-42.338	-2.3	16.67
	Tertiary	-10.501	1.5	4.030
Sim, HAZ 110°C	Primary	-63.475	-2.183	26.14
	Tertiary	-23.600	1.965	10.04

Table 4 Equations (3) and (4) constants determined in the analysis of uniaxial creep curves

Structure Temperature Constant	PM 75°C	PM 110°C	PM 145°C	WM 110°C	Sim. HAZ 110°C
a_0	-9.640	14.74	-12.29	-12.14	-19.90
a_1	3.561	6.095	4.988	4.831	8.266
a_2	.2094	2533	.3254	.2417	.3114
b_0	$1.31 \cdot 10^{-3}$	$5.07 \cdot 10^{-3}$	$5.20 \cdot 10^{-3}$	$3.36 \cdot 10^{-4}$	$1.51 \cdot 10^{-4}$
b_1	.0392	.0125	.00984	.0332	.0358
b_2	$1.90 \cdot 10^{-22}$	$4.64 \cdot 10^{-21}$	$2.97 \cdot 10^{-28}$	$9.80 \cdot 10^{-24}$	$4.60 \cdot 10^{-22}$
b_3	1	1	1	1	1
b_4	9.28	9.55	13.46	11.04	9.46
b_5	$1.40 \cdot 10^{-10}$	$1.11 \cdot 10^{-11}$	$2.14 \cdot 10^{-10}$	$2.56 \cdot 10^{-11}$	$8.83 \cdot 10^{-13}$
b_6	.0713	.124	.124	.134	.127

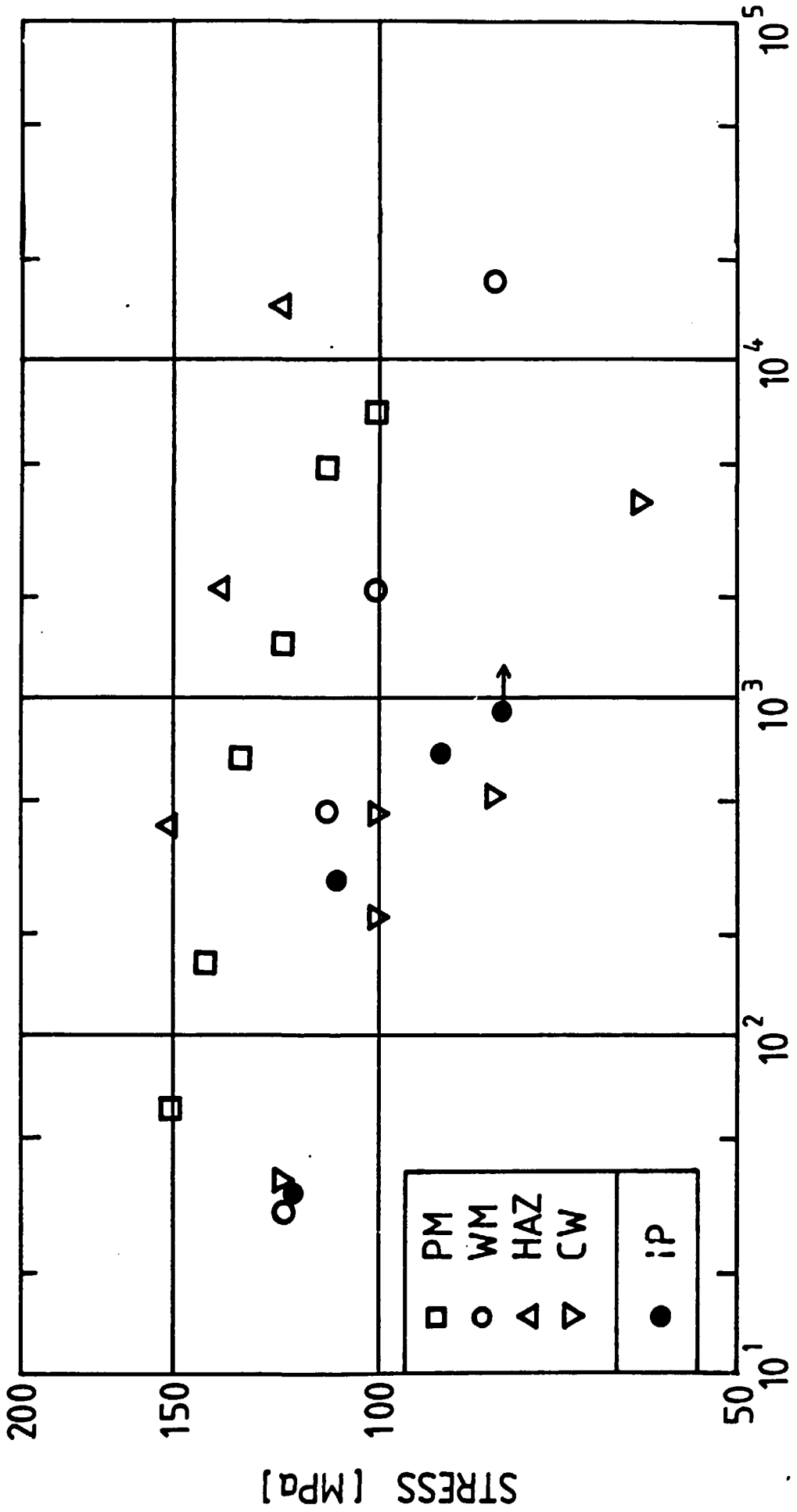

Fig. 1 Stress vs. rupture time for parent metal (PM), weld metal (WM), simulated HAZ (HAZ), and cross-weld (CW) specimens tested at 110°C. Rupture times for internal pressure tested tubes (IP) are plotted vs. maximum sress.

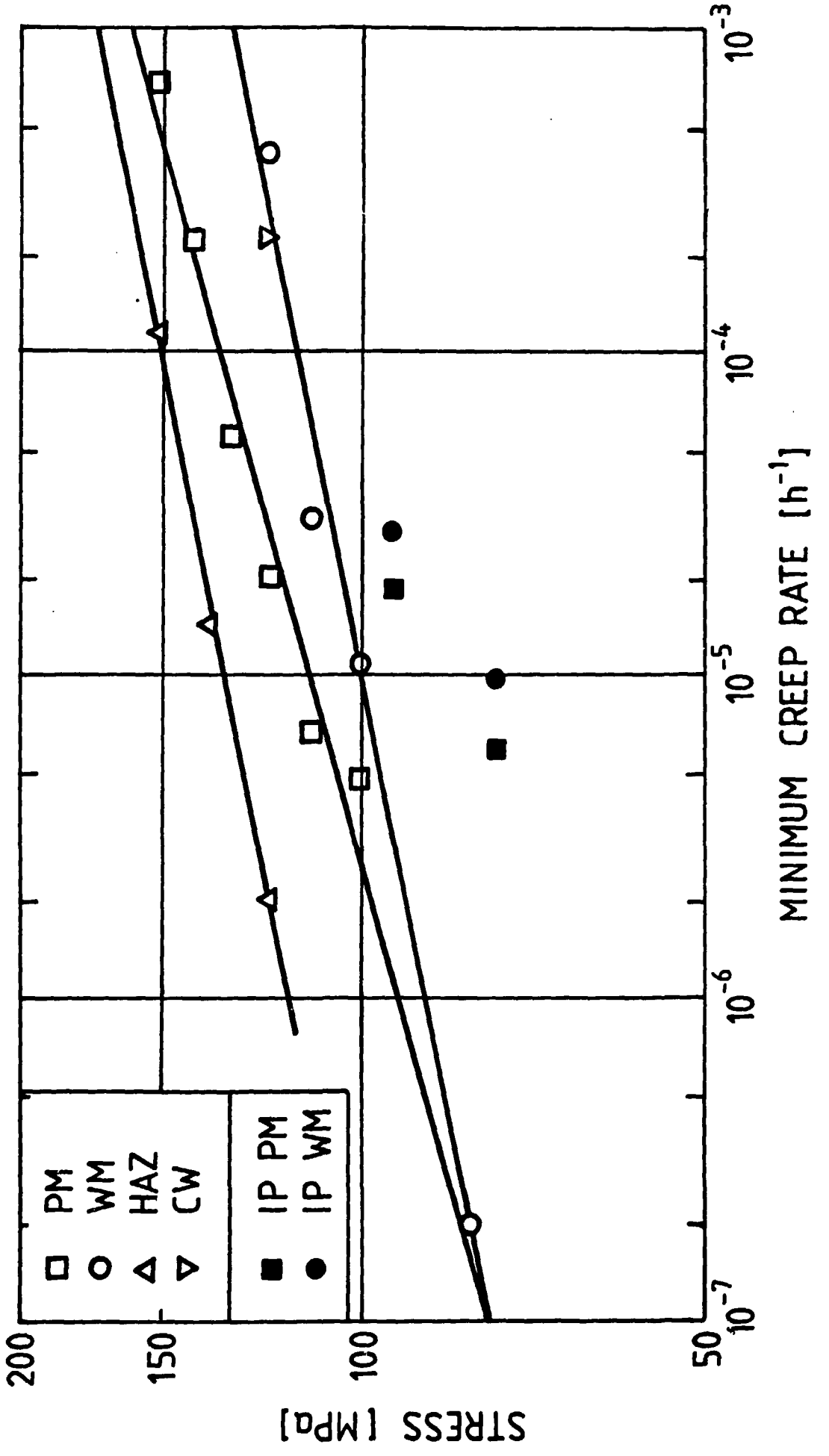

Fig. 2 Stress vs. minimum creep rate for parent metal (PM), weld metal (WM), simulated HAZ (HAZ), and cross-weld (CW) specimens tested at 110°C. Creep rates for internal pressure tested tubes (IP) are plotted vs. effective stress.

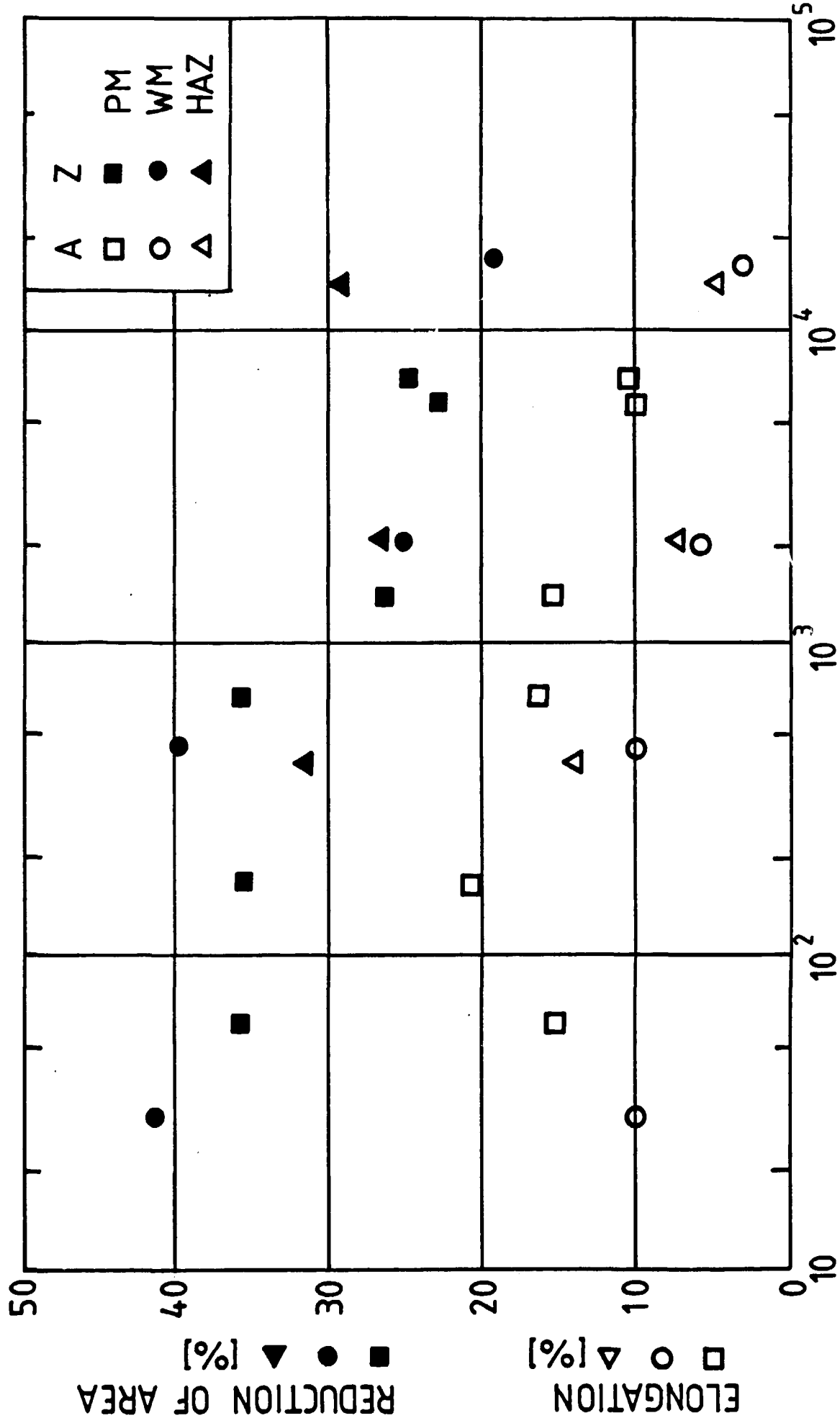

Fig. 3 Elongation and reduction of area vs. rupture time for parent metal (PM), weld metal (WM), and simulated HAZ (HAZ) specimens tested at

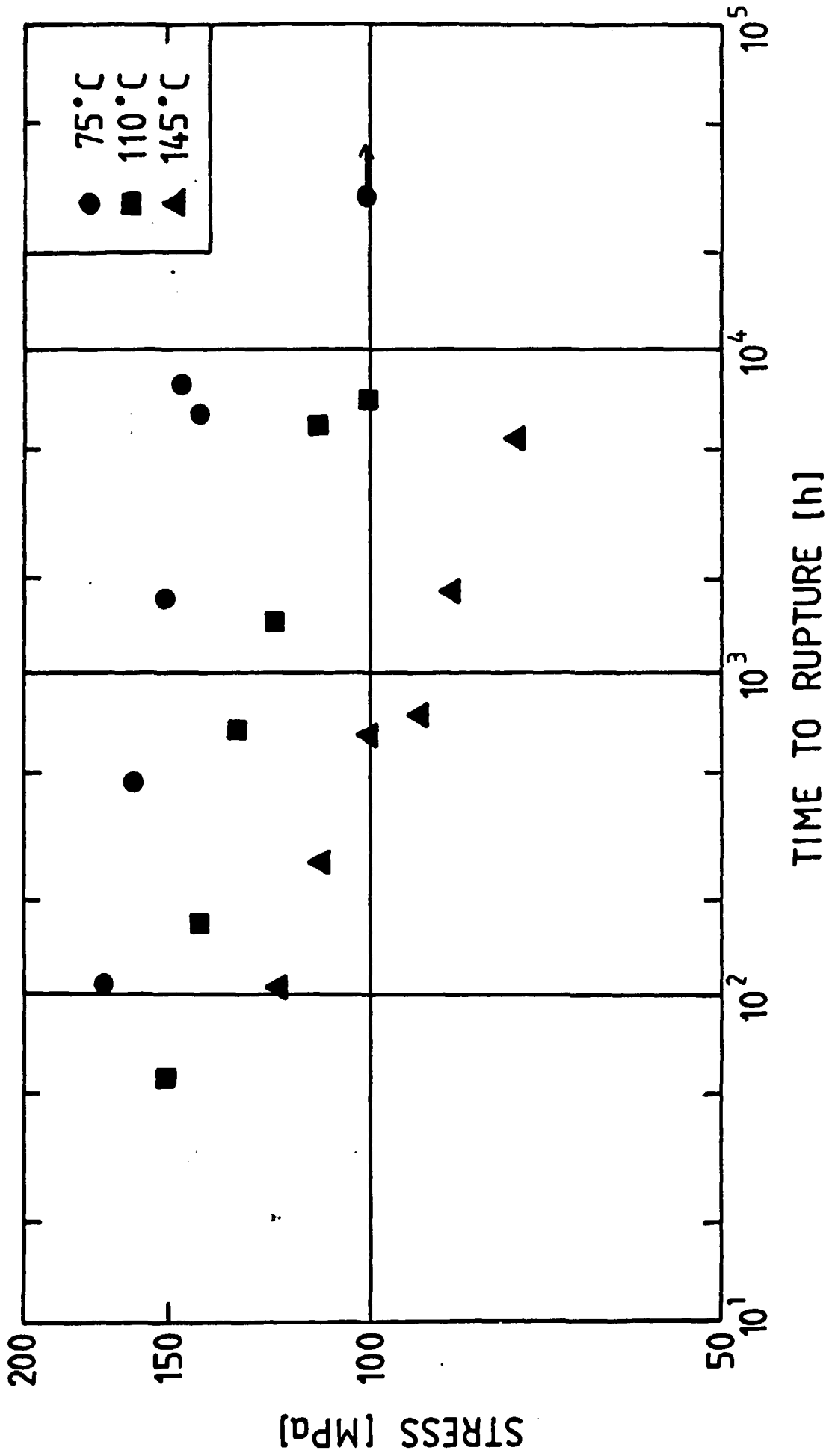

Fig. 4 Stress vs. rupture time for parent metal tested at 75, 110, and 145°C.

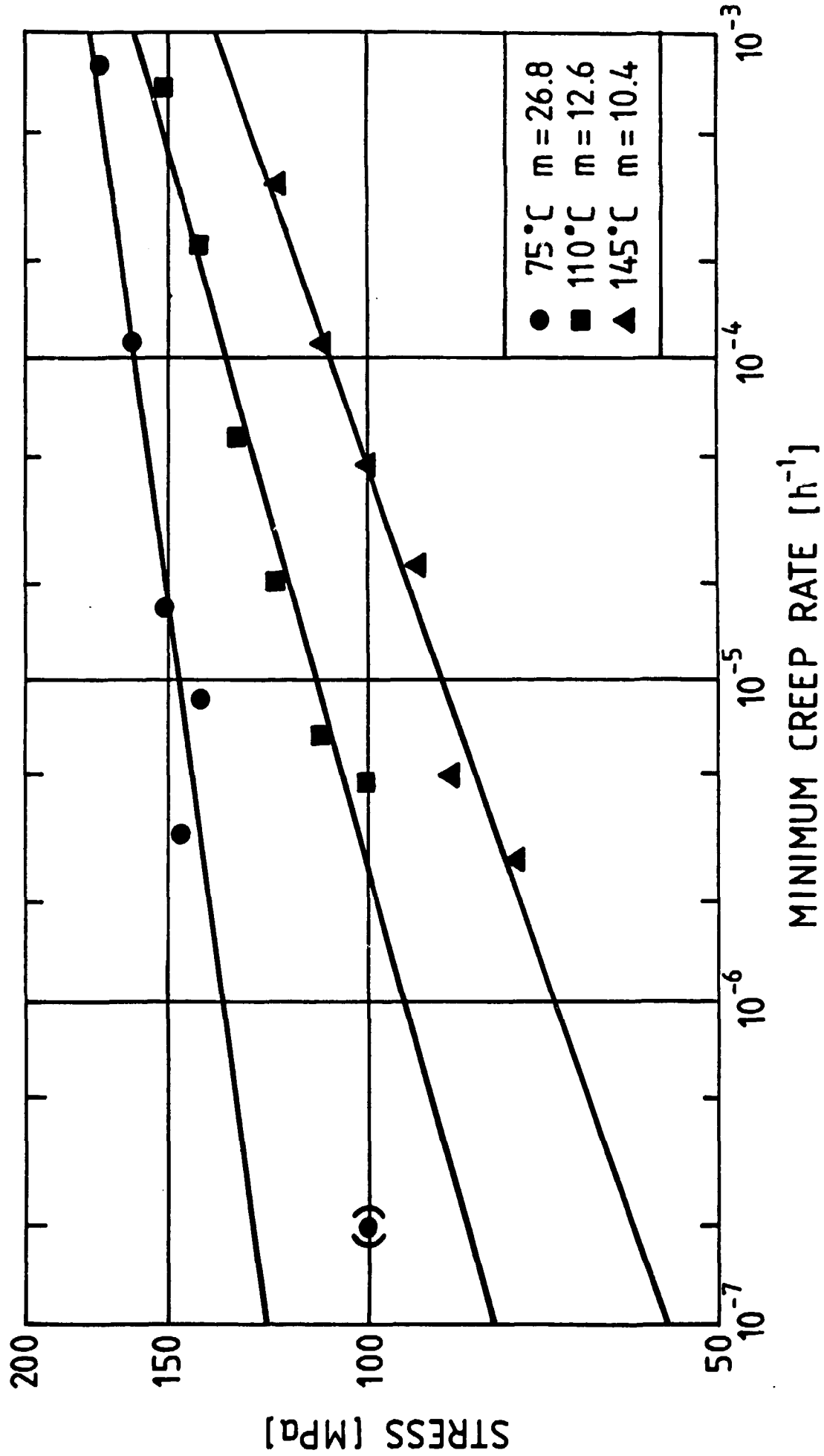

Fig. 5 Stress vs. minimum creep rate for parent metal tested at 75, 110, and 145°C.

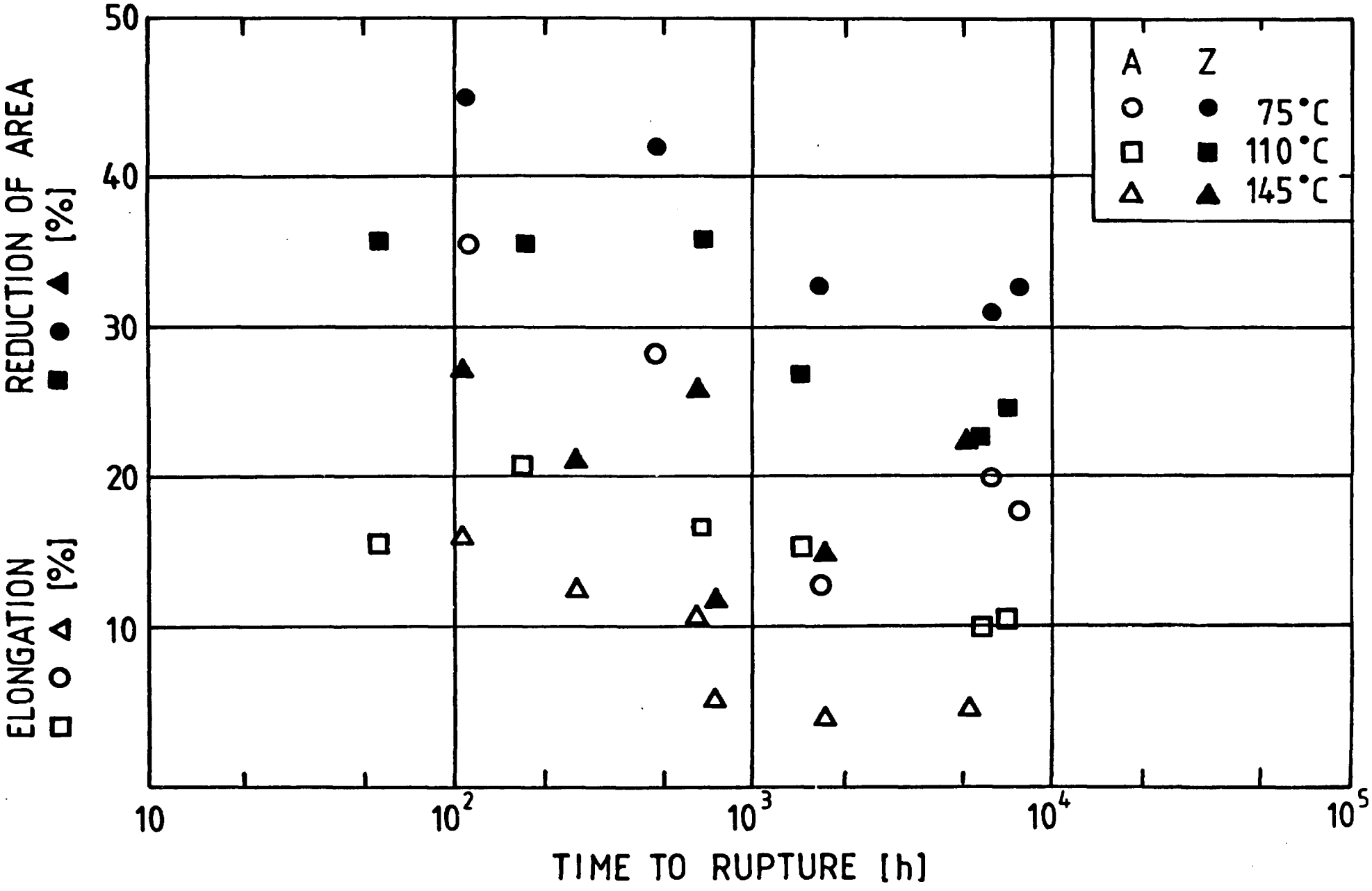

Fig. 6 Elongation and reduction of area vs. rupture time for parent metal tested at 75, 110, and

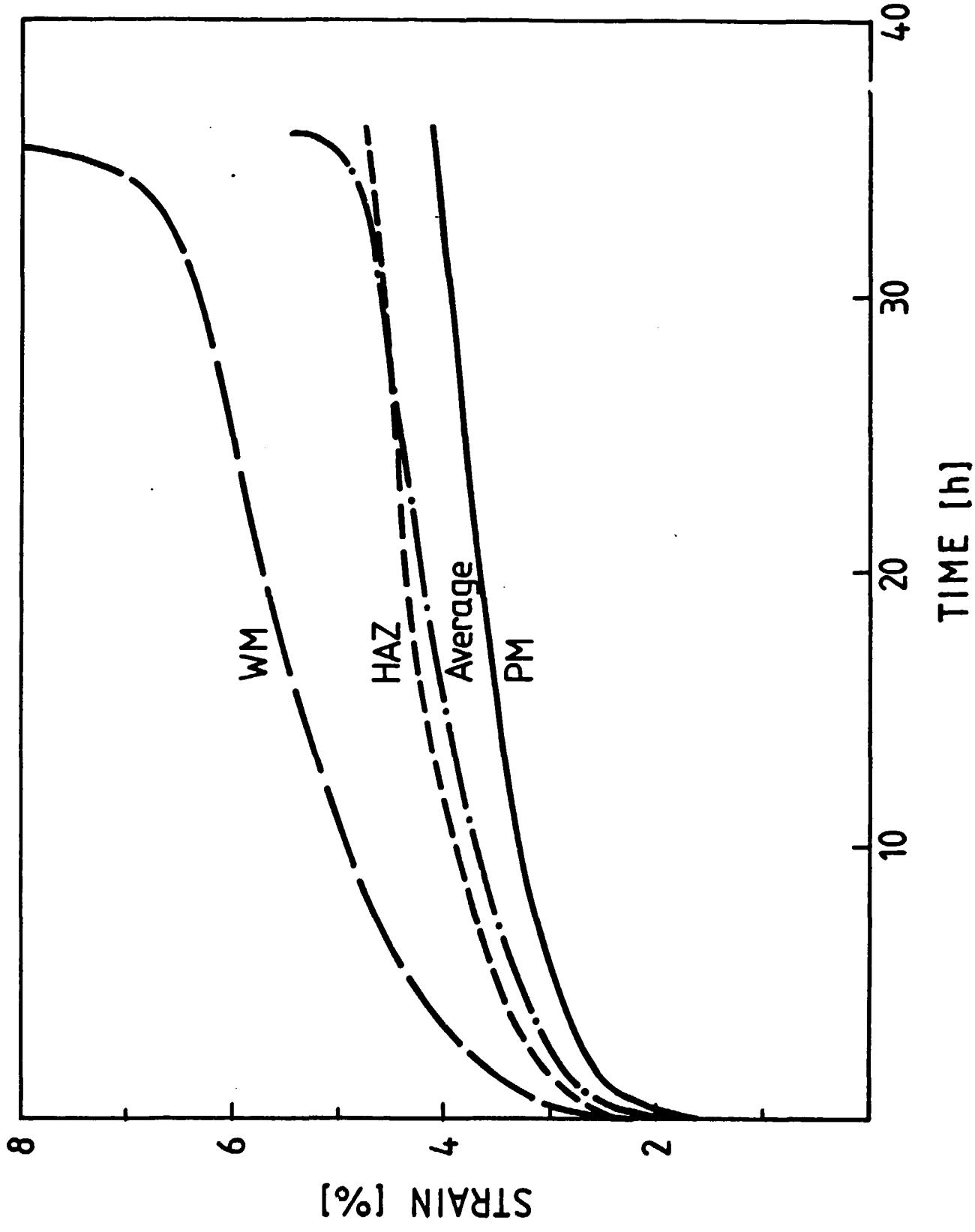

Fig. 7 Creep curves for the parent metal (PM), weld metal (WM), and HAZ structures in a cross-weld specimen tested at 110°C, 120 MPa. An average creep curve is included.

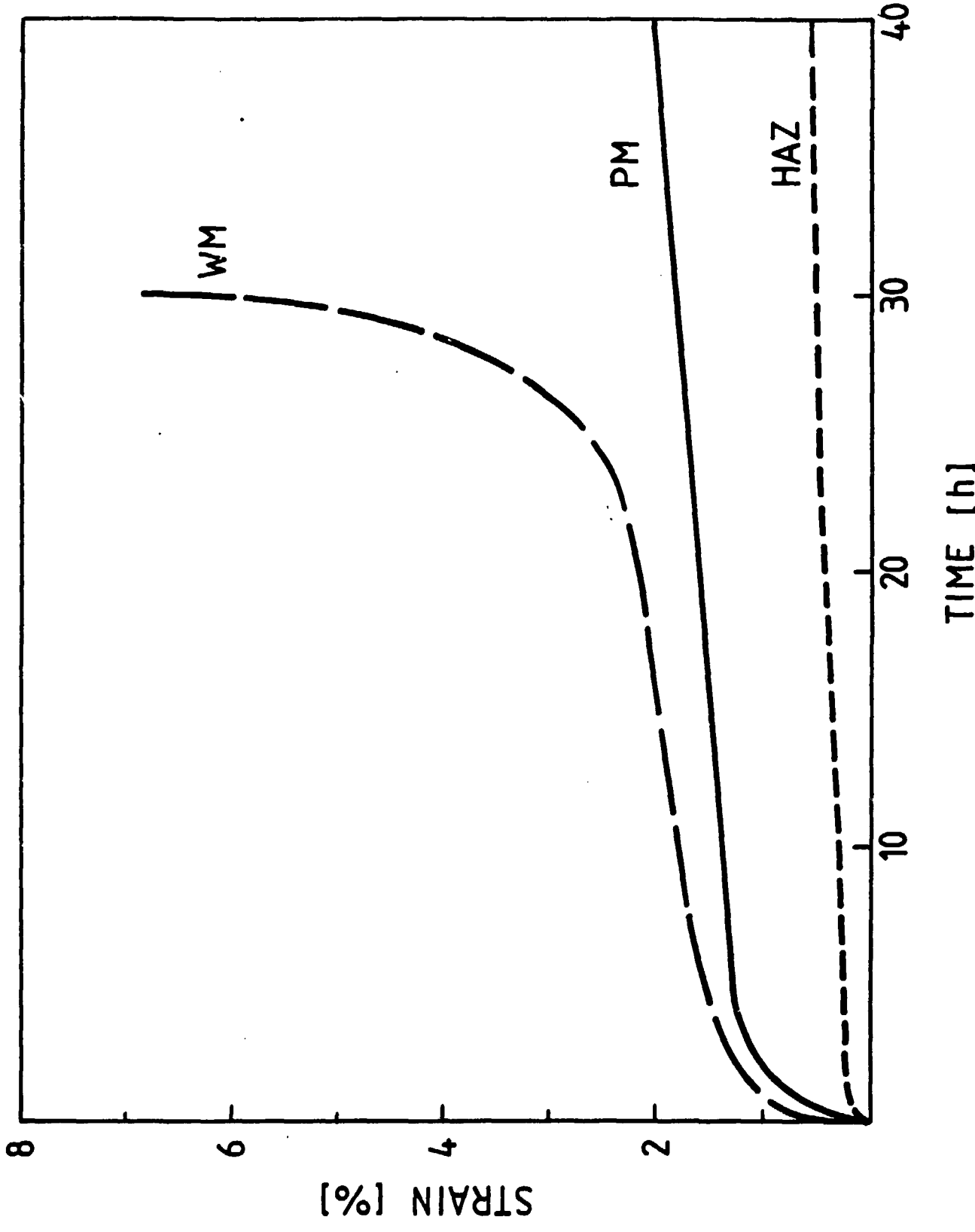

Fig. 8 Uniaxially determined creep curves for parent metal (PM), weld metal (WM), and simulated HAZ tested at 110°C, 120 MPa. Cf Fig. 7.

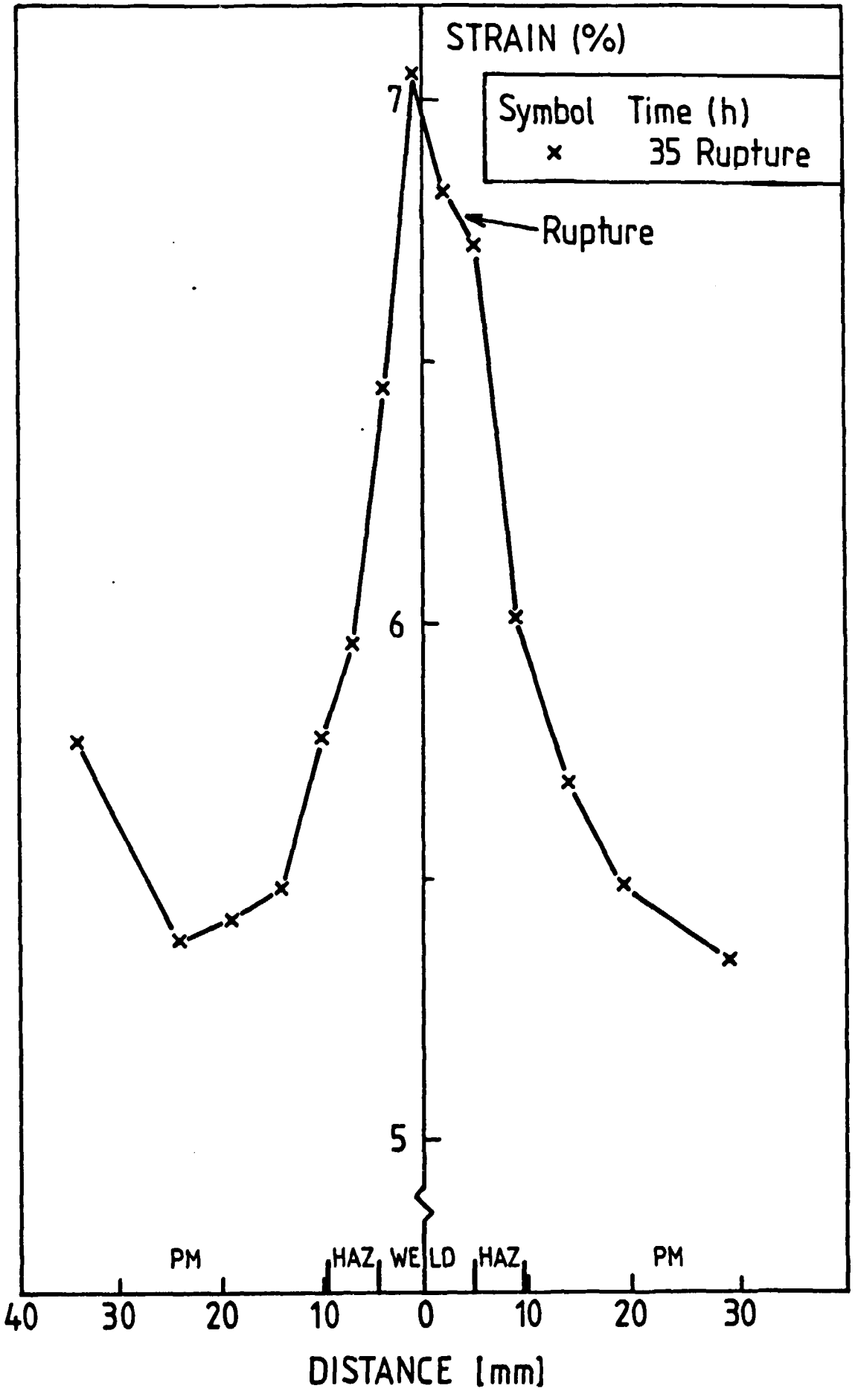

Fig. 9 Strain distribution along an internal pressure tested tube, 400-2, at rupture.

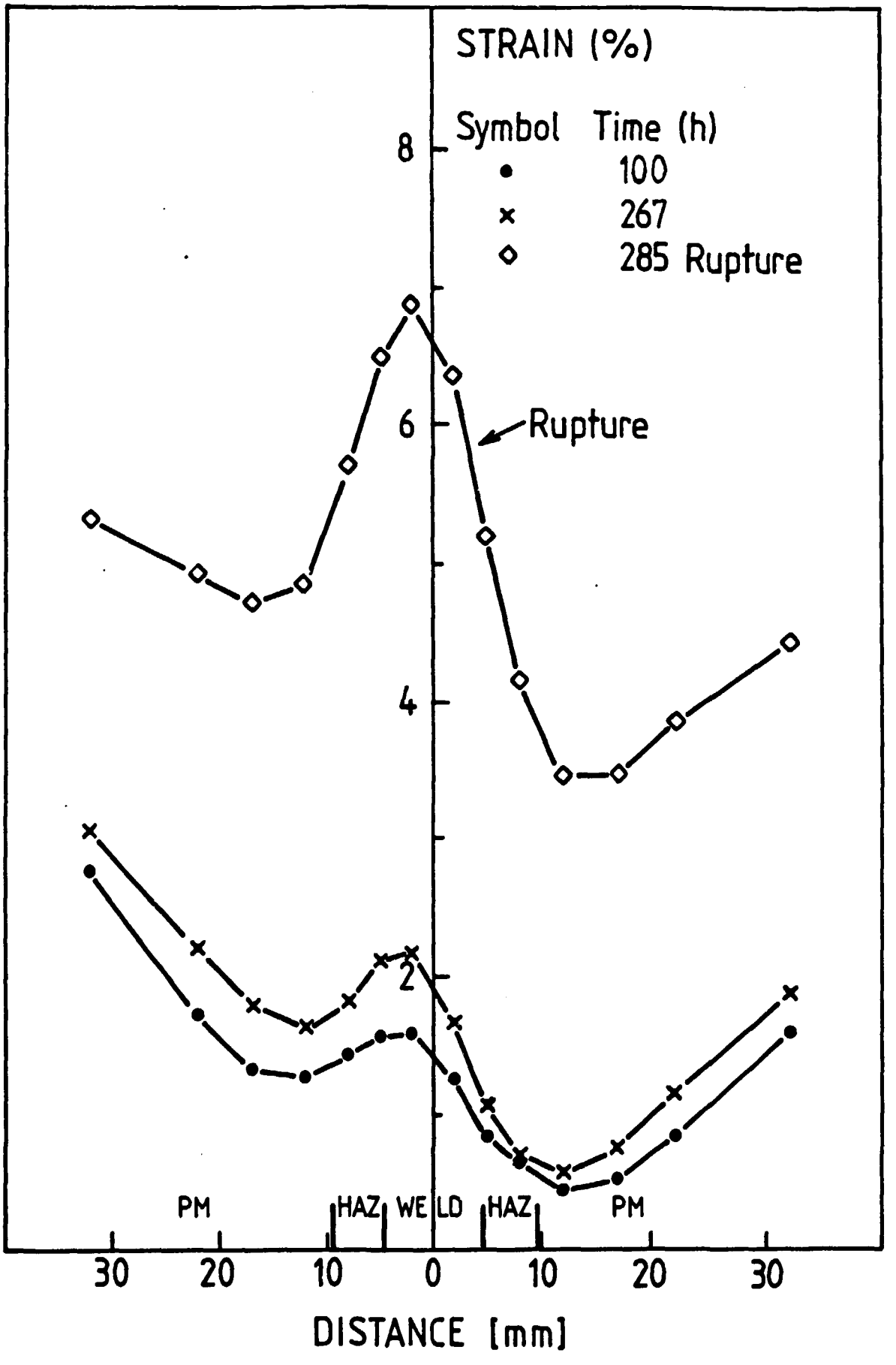

Fig. 10 Strain distribution along an internal pressure tested tube, 4, at various times and at rupture.

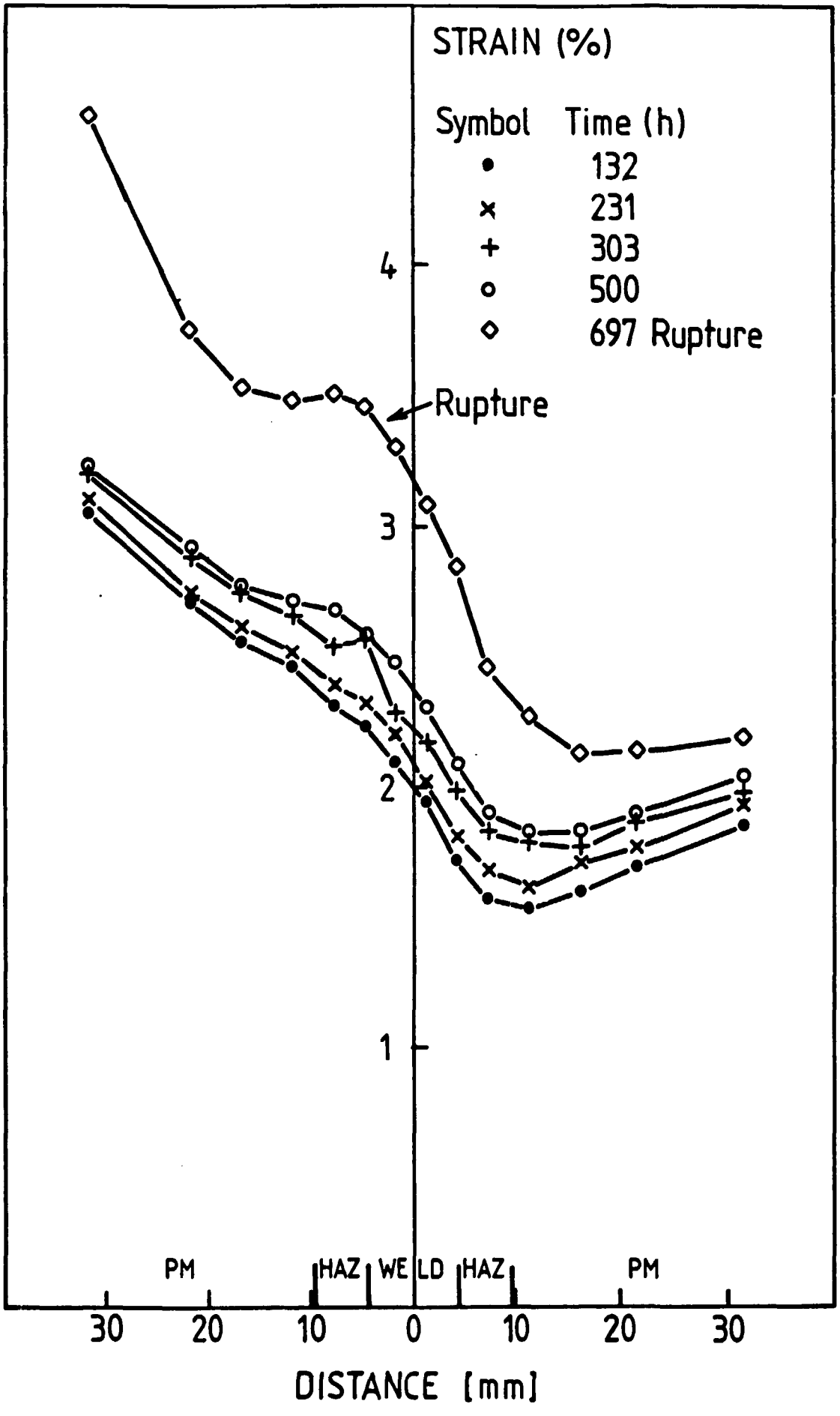

Fig. 11 Strain distribution along an internal pressure tested tube, 300-1, at various times and at rupture.

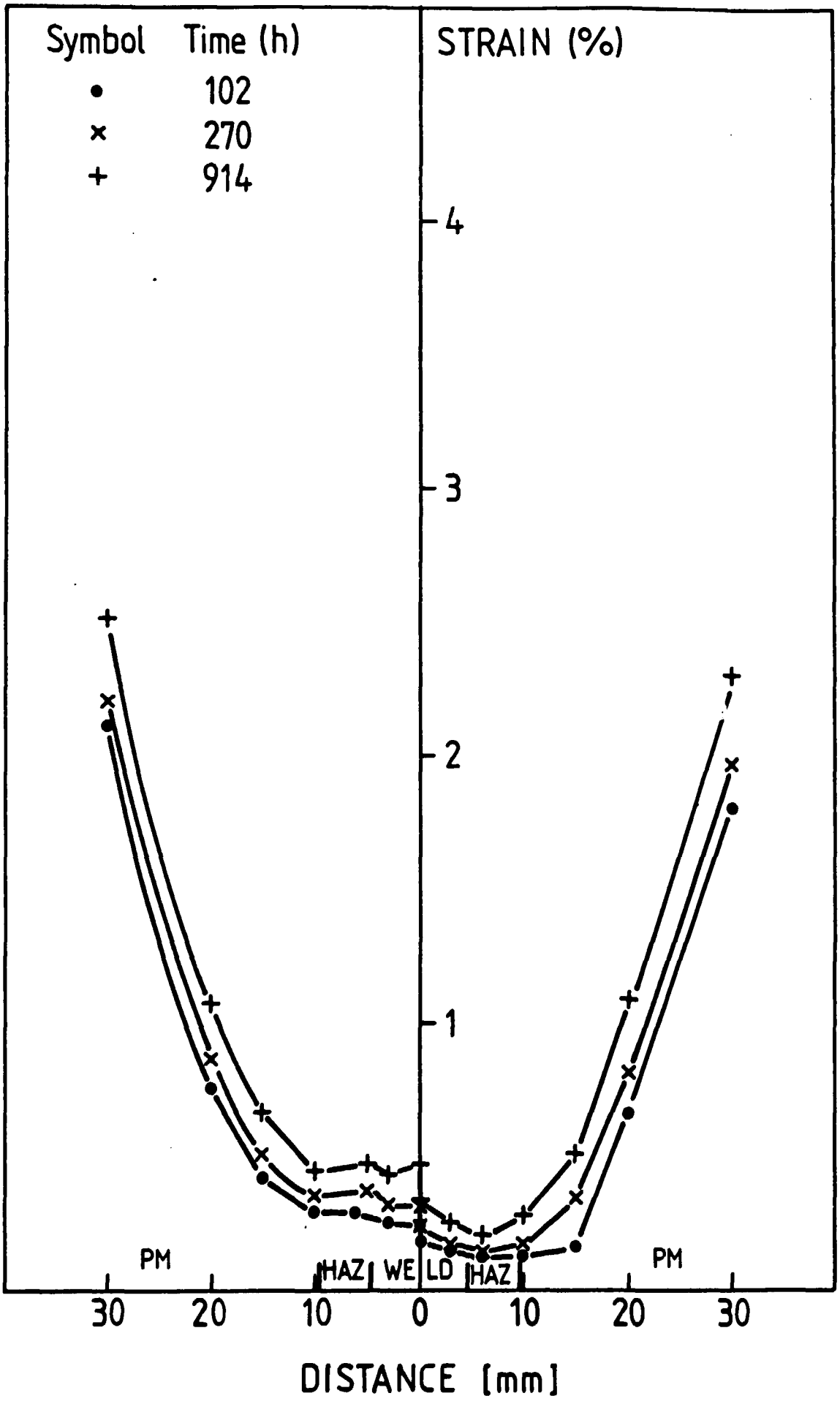

Fig. 12 Strain distribution along an internal pressure tested tube, 5, at various times. Testing still in progress.

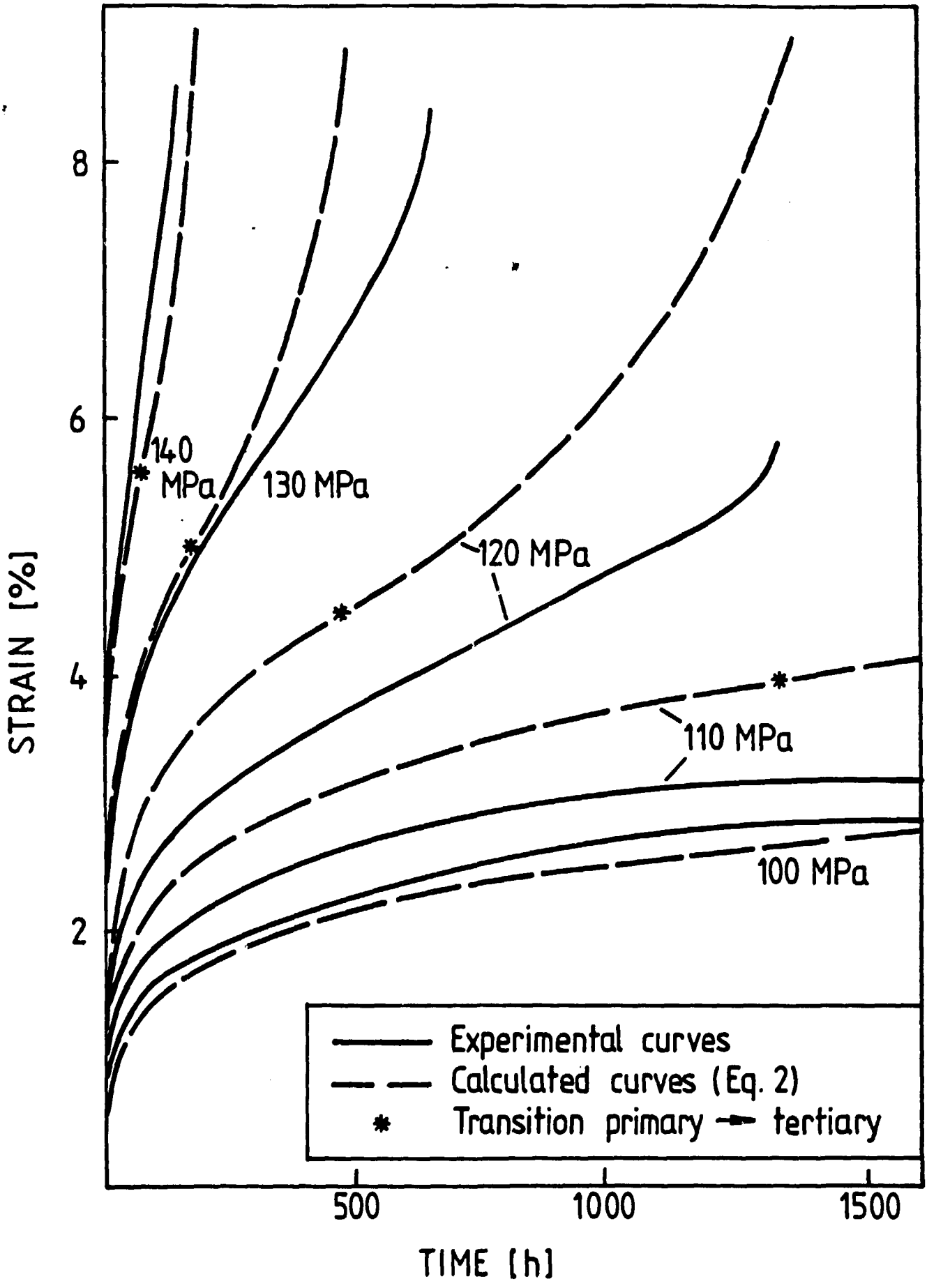

Fig. 13 Comparison between experimental and Equation (2) creep curves for parent metal tested at 110°C.

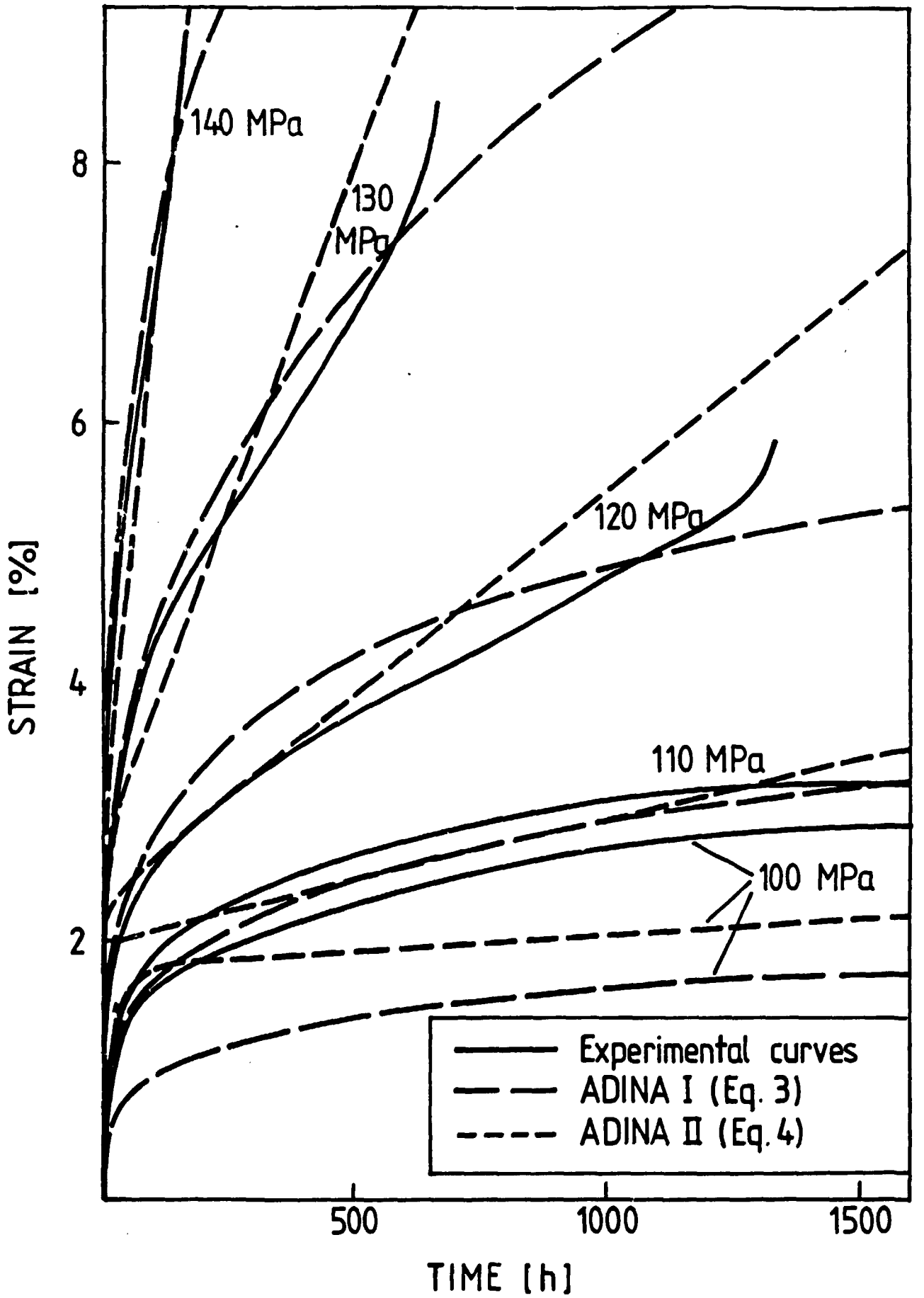

Fig. 14 Comparison between experimental and Equations (3) and (4) creep curves for parent metal tested at 110°C.

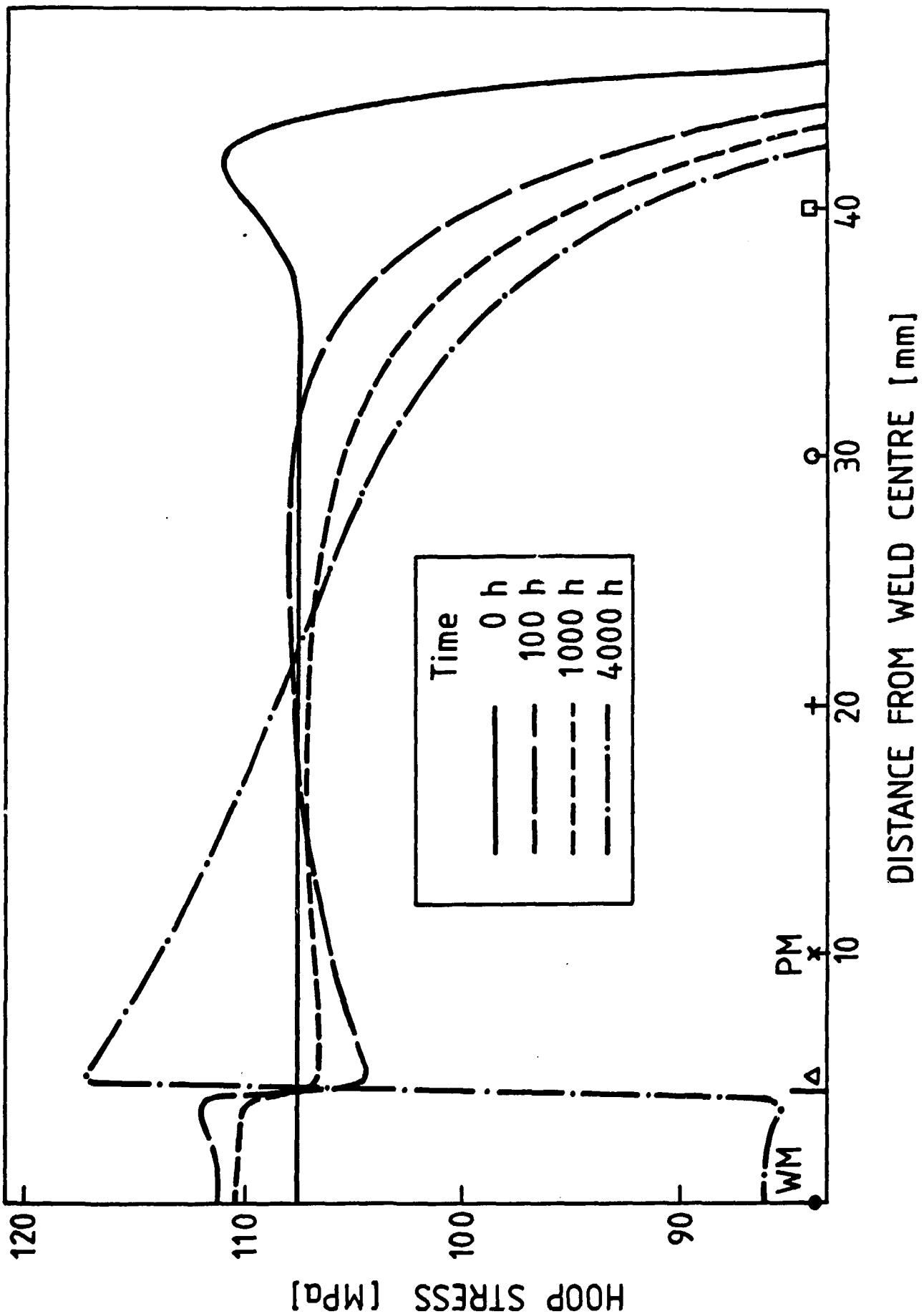

Fig. 15a Calculated hoop stress distribution along an internal pressure tested tube at various times. Tube 4. No HAZ.

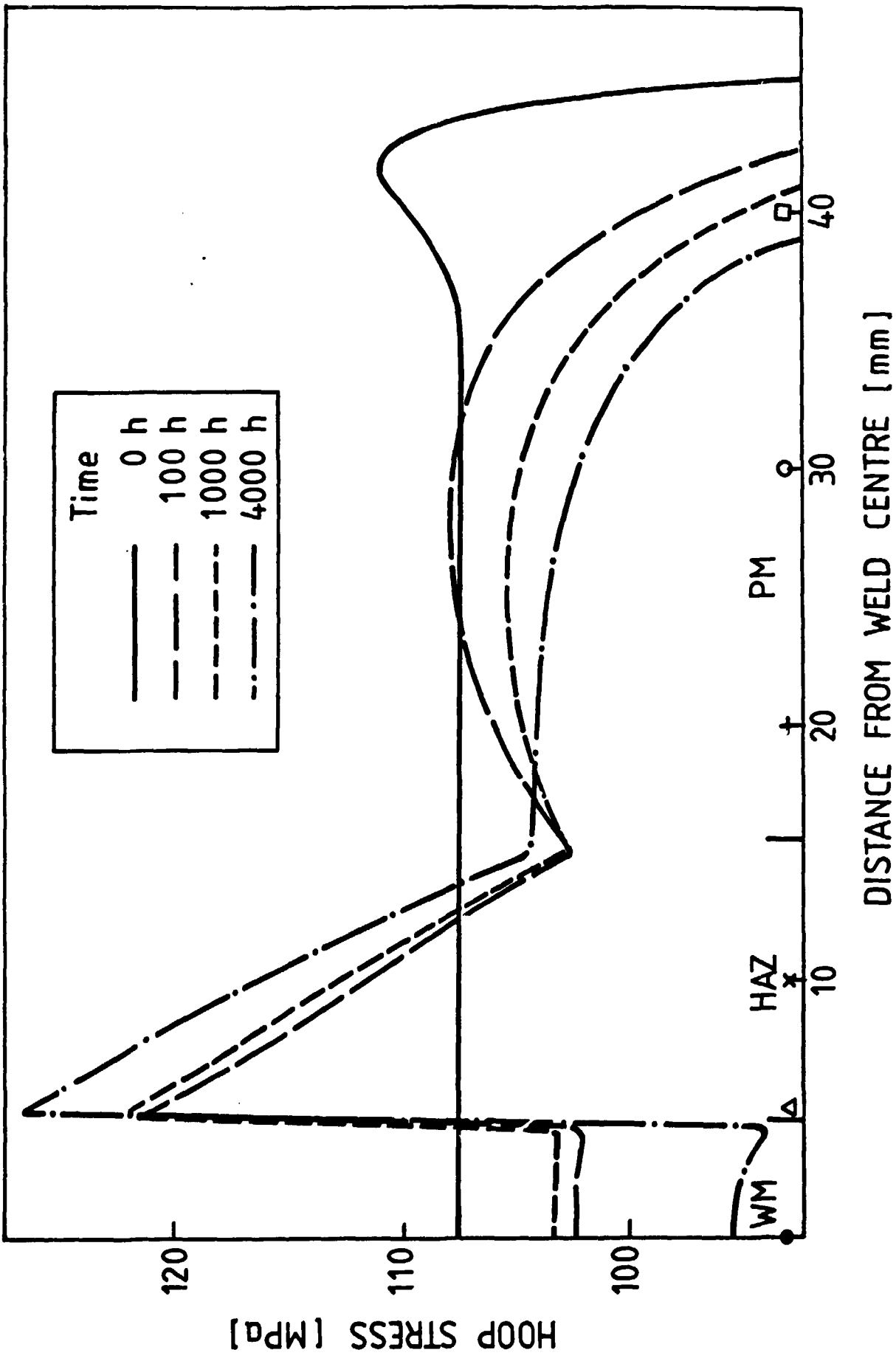

Fig. 15b Calculated hoop stress distribution along an internal pressure tested tube at various times. Tube 4. Modified HAZ.

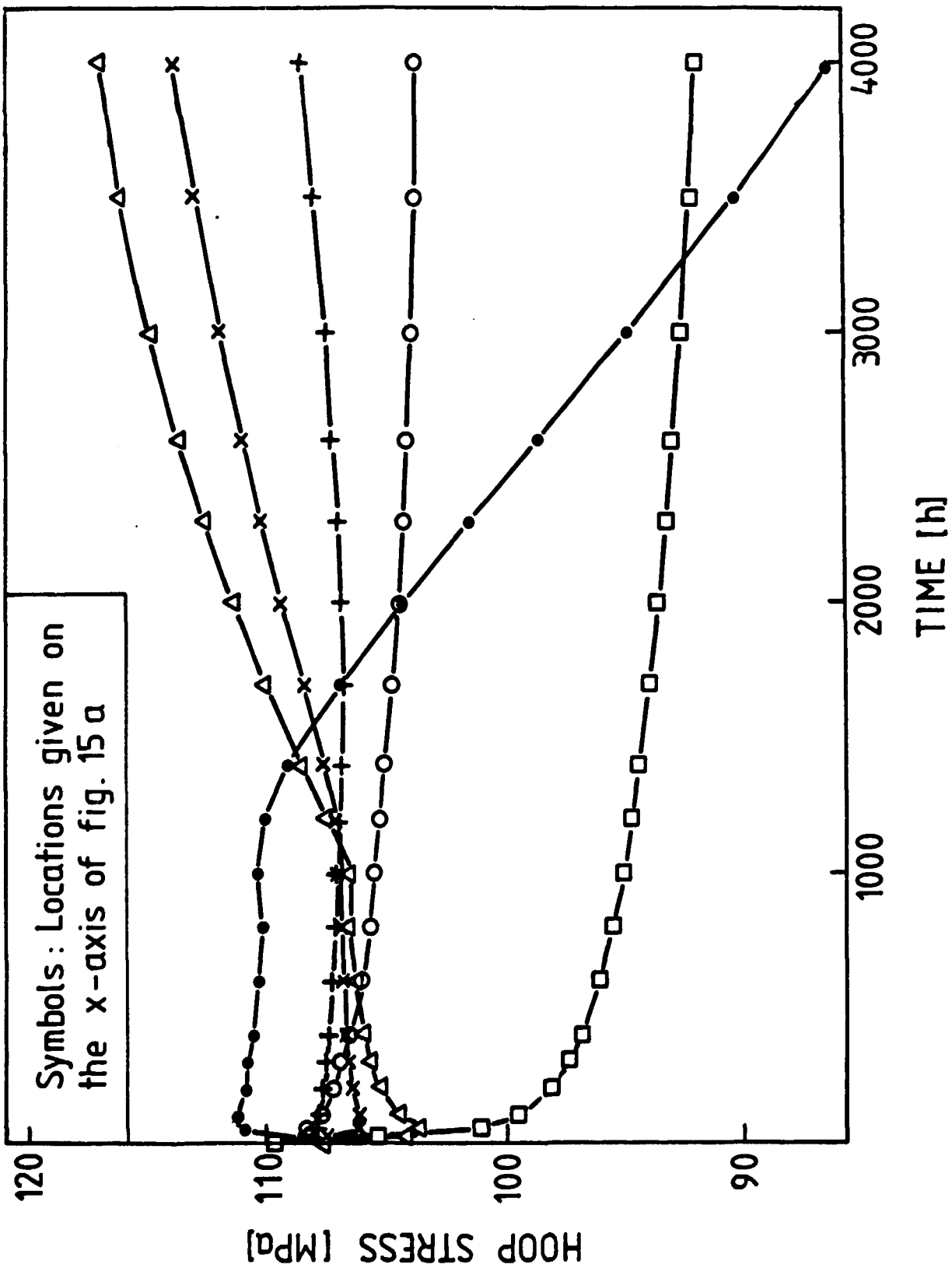

Fig. 16a Calculated time variation of hoop stress at different locations in an internal pressure tested tube. Tube 4. No HAZ.

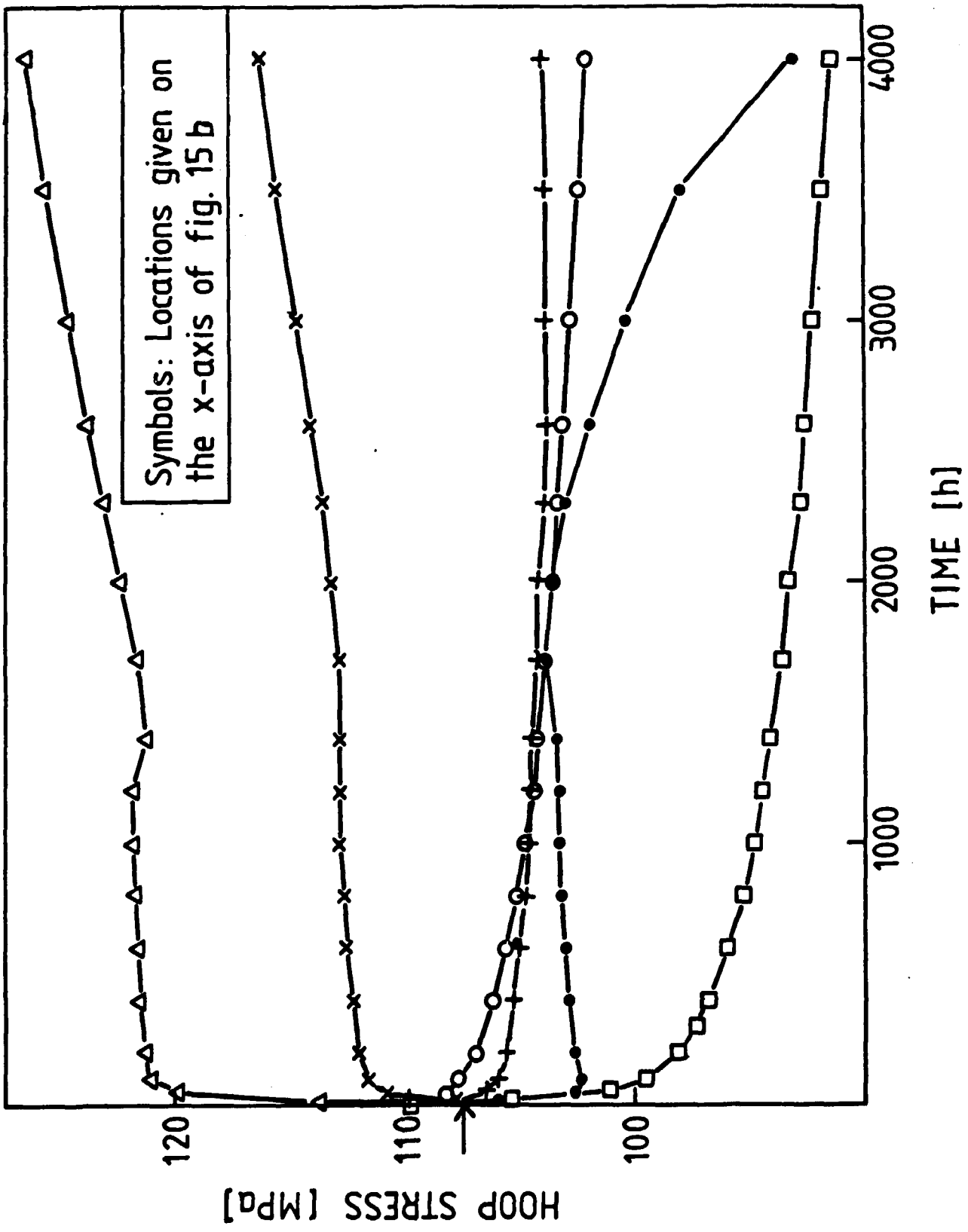

Fig. 16b Calculated time variation of hoop stress at different locations in an internal pressure tested tube. Tube 4. Modified HAZ.

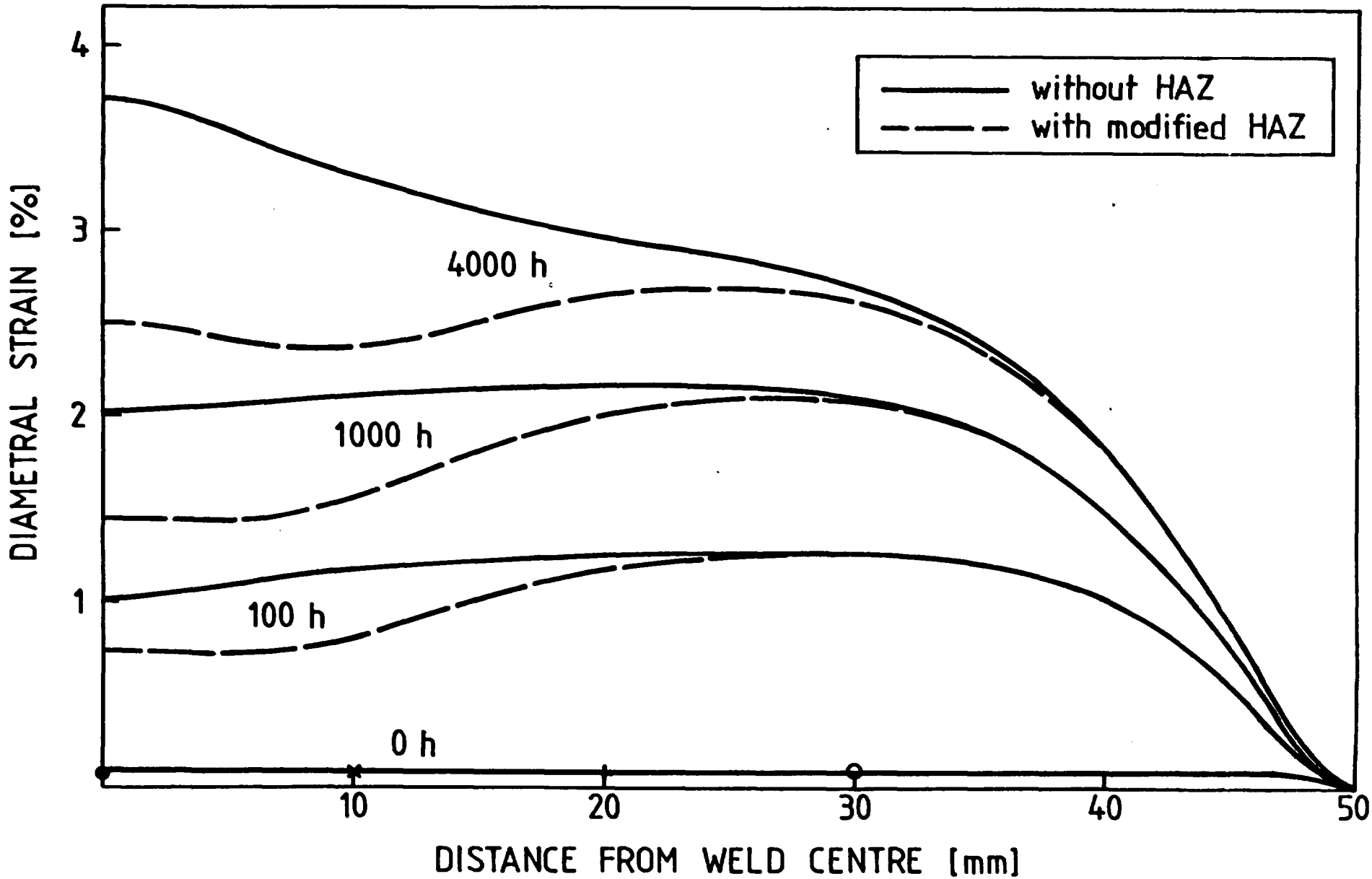

Fig. 17 Calculated diametral strain distribution along an internal pressure tested tube at various times. Tube 4. No HAZ and modified HAZ.

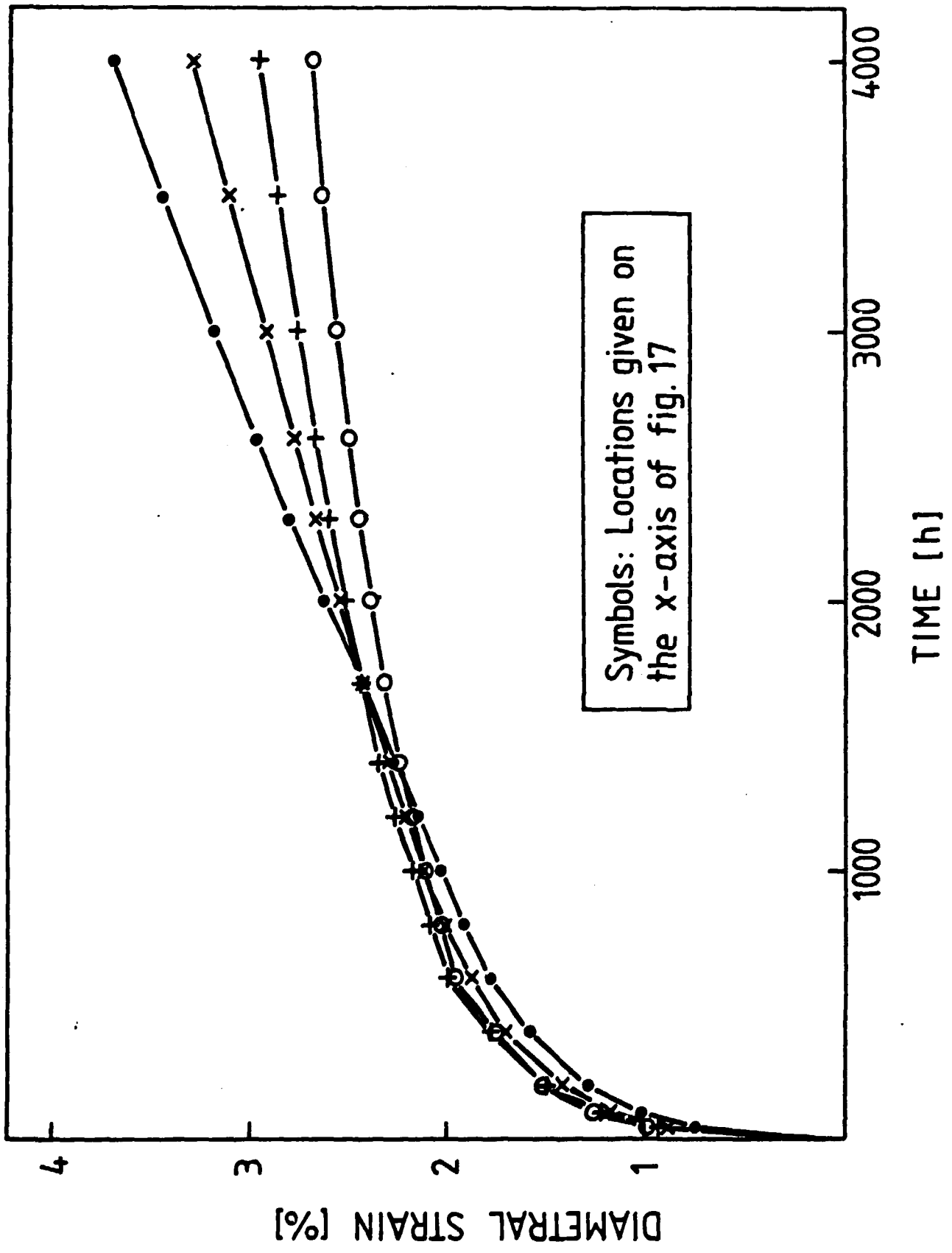

Fig. 18a Calculated time variation of diametral strain at different locations in an internal pressure tested tube. Tube 4. No HAZ.

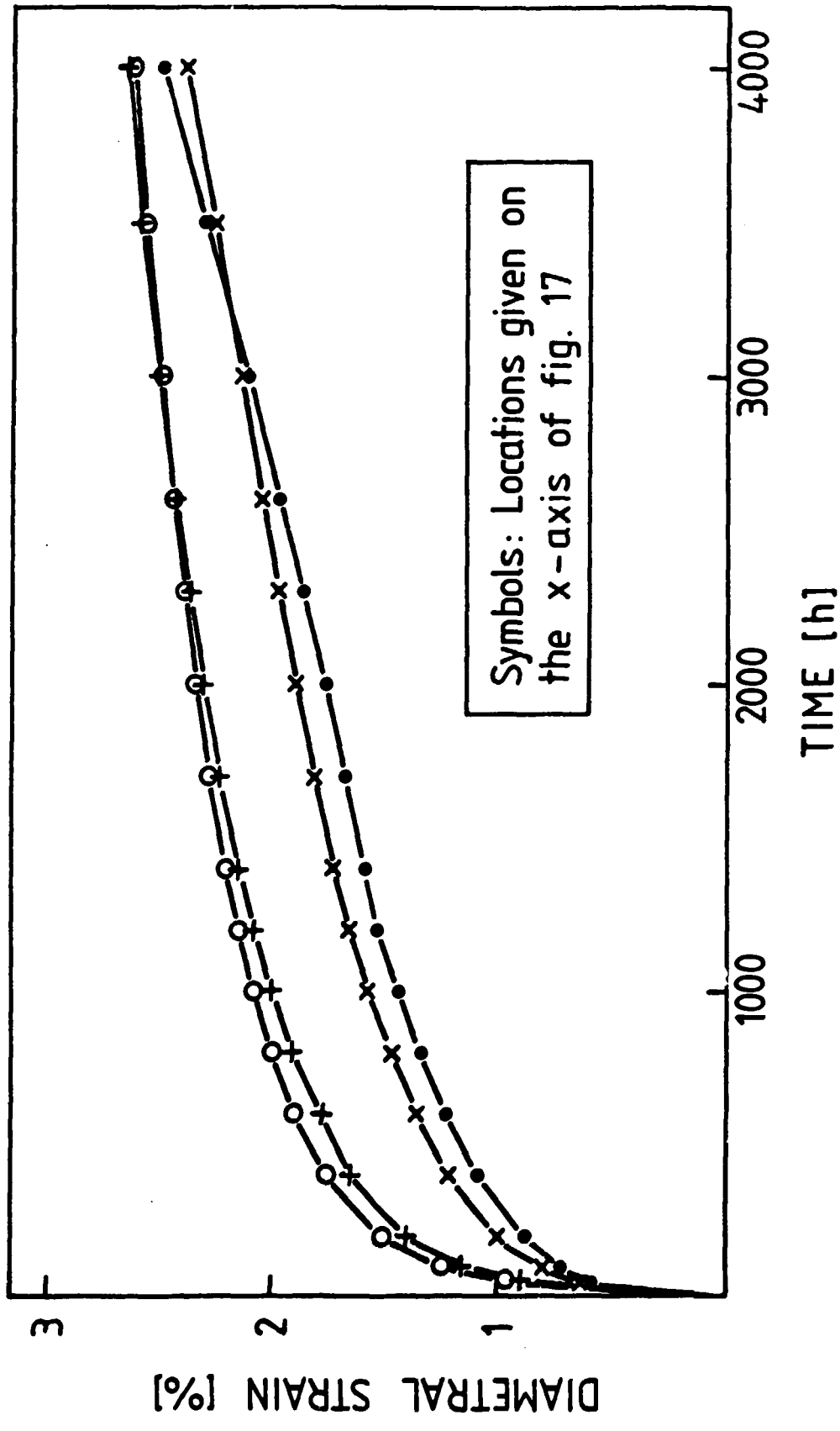

Fig. 18b Calculated time variation of diametral strain at different locations in an internal pressure tested tube. Tube 4. Modified HAZ.

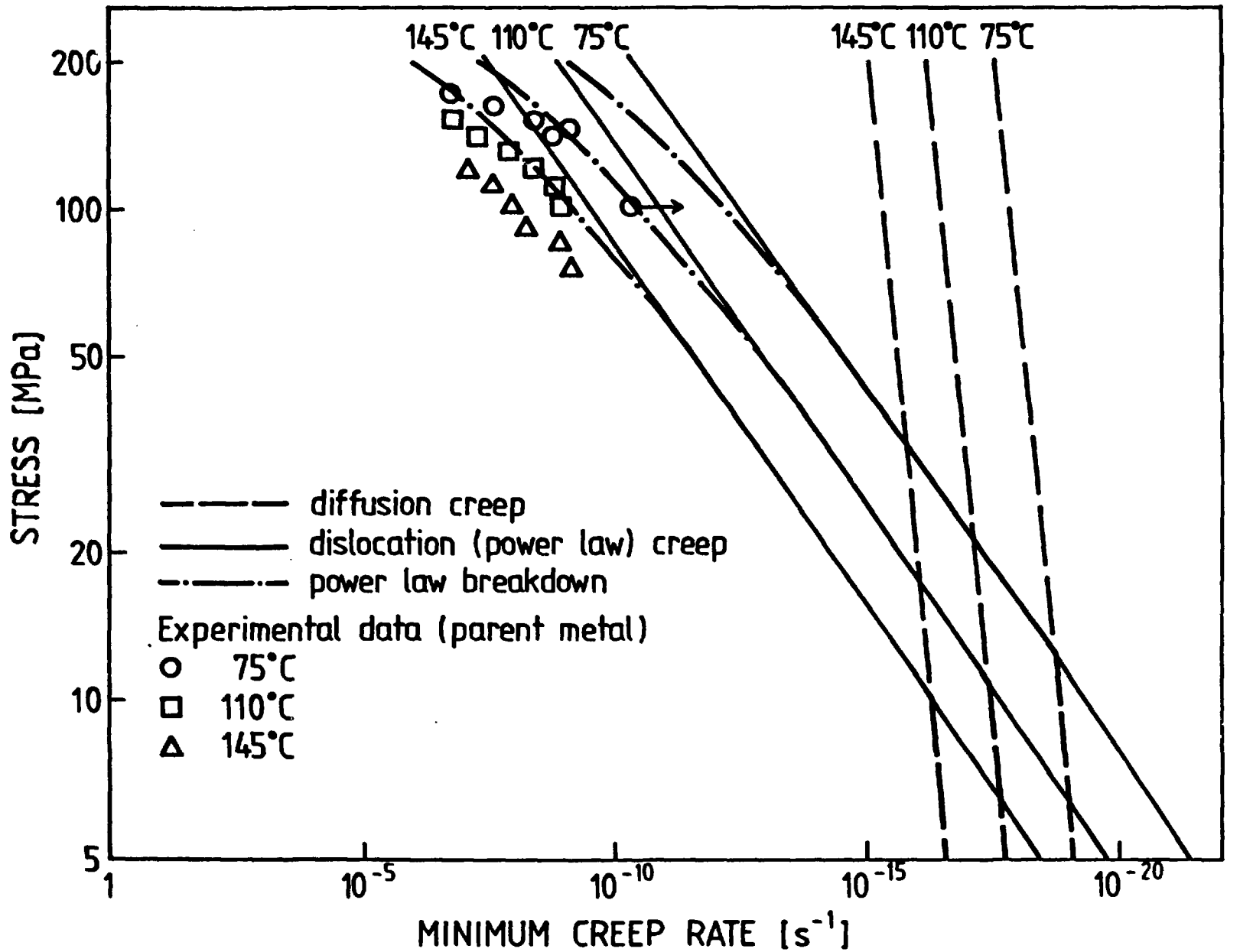

Fig. 19 Theoretical stress dependence of the minimum creep rate at 75, 110, and 145°C derived from equations and materials data given in Ref. 10. Comparison with experimental values.

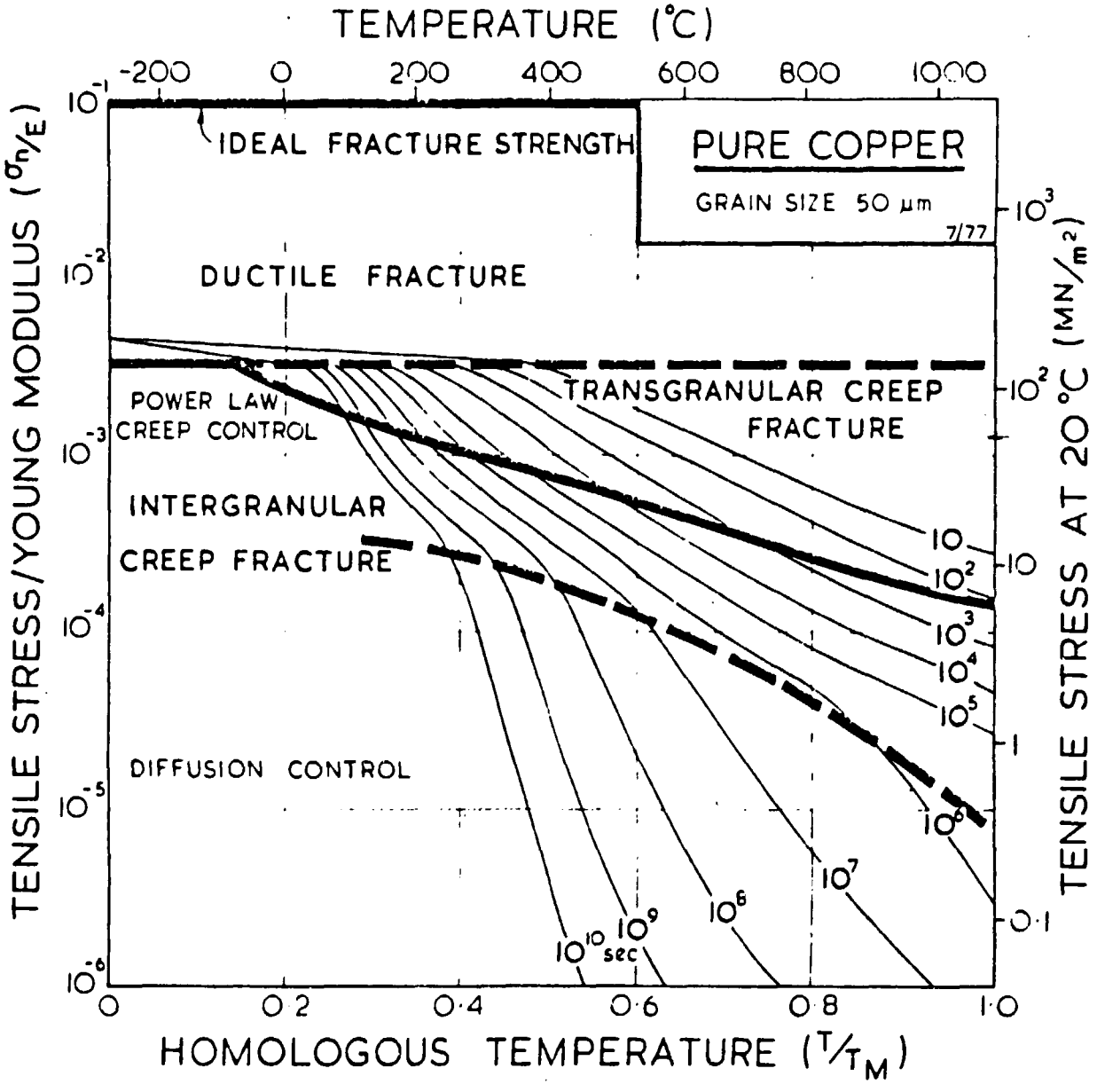

Fig. 20 Fracture mechanism map reproduced from Ref. 11.

APPENDIX A. CONSTITUTIVE EQUATIONS DESCRIBING ENTIRE CREEP CURVES.

In the computer simulations of the creep behaviour of the welded tubes a program, developed for calculation of creep deformation and buckling of arbitrary axisymmetric shells, Ref. A1, has been used. In this program the creep behaviour is characterized by the coefficients B and n in the Norton expression

$$\dot{\varepsilon} = B \cdot \sigma^n \qquad \text{(A1)}$$

These coefficients have been determined from uniaxial creep test results for different structures in the welded joint.

In the analyses for a cold-worked AISI 316 stainless steel the coefficients were thus varied along the tube. In the first calculations, Ref. A2, only secondary creep rates were used i.e. B and n were not dependent on strain or time. These calculations resulted in excellent predictions of time to and location of rupture but the deformation was considerably underestimated.

In refined calculations, Ref. A3, primary creep was accounted for by the introduction of time dependent coefficients B and n. These calculations gave good descriptions of the deformation behaviour without loss of accuracy in the predictions of where and when rupture was to occur. However, the constitutive equation used to represent the uniaxial creep behaviour was only successful in describing the primary and to some extent the secondary creep stages (see Ref. A3, Fig. 2). In the AISI 316 calculations this fact was regarded as less important since tertiary creep was practically non-existent in the cold-worked material.

But in more ductile materials, as in this investigation,

tertiary creep is more important and can even be the dominating stage of the creep life. Therefore a different constitutive equation in which tertiary creep is accounted for has had to be developed. Due to the limitations imposed by the use of the Norton equation in the computer program, a single equation cannot be used to describe an entire creep curve. Thus, at least two sets of Norton coefficients are required.

As pointed out in Ref. A3 somewhat better results should be achieved if a strain dependent - instead of time dependent - creep rate was applied in the calculations. Since good correlations between creep strain and creep rate were found for tertiary creep of low alloy steels, Ref A4, similar evaluations, extended to include primary creep, were performed for the uniaxial creep test results for the structures tested in this investigation.

In Fig. A1 a typical plot of log (creep rate) against creep strain is shown. It is obvious that two straight lines can be fitted to the data for every test. The corresponding equation is:

$$\log \dot{\varepsilon} = a + b \cdot \varepsilon, \qquad \text{(A2)}$$

where b is negative for primary and positive for tertiary creep. (Of course an intermediate secondary creep region with constant creep rate can be included, but as a rule this region is rather small and has hence been disregarded.)

The results from tests at different stresses can be summarized in one equation by the introduction of stress dependent coefficients a and b in Eq. (A2):

$$\log \dot{\varepsilon} = c + d \cdot \log\sigma + (e + f \cdot \log \sigma) \cdot \varepsilon, \qquad \text{(A3)}$$

with different c, d, e, and f values for primary and tertiary creep.

These four constants for each creep stage and structure are determined simultaneously by regression analysis. In a few cases this has led to less satisfactory fit to the results of a single test - especially for the tertiary stage where the scatter can be considerable.

Eq. (A3) can be rewritten as:

$$\log \dot{\varepsilon} = c + e \cdot \varepsilon + (d + f \cdot \varepsilon) \cdot \log\sigma$$

$$\dot{\varepsilon} = 10^{(c + e\cdot\varepsilon)} \cdot \sigma^{(d + f\cdot\varepsilon)} \qquad \text{(A4)}$$

i.e. the Norton equation (A1), with strain dependent coefficient.

Besides the different sets of four constants (c, d, e, and f), the "point" of transition from primary to tertiary creep has to be known by the computer, and is determined in the following way:

Eq. (A3) is simplified to:

$$\dot{\varepsilon} = C_p \cdot e^{D_p \cdot \varepsilon} \qquad \text{(A5)}$$

and $$\dot{\varepsilon} = C_t \cdot e^{D_t \cdot \varepsilon}, \qquad \text{(A6)}$$

where $C = 10^{(c + d \log \sigma)}$

and $D = \ln 10 \cdot (e + f \cdot \log\sigma)$,

and the subscripts p and t denote primary and tertiary creep respectively. (D_p is negative and D_t positive.)

Eq. (A5) represent a strain rate which decreases with increasing strain while the Eq. (A6) strain rate increases. The primary - tertiary transition occurs for the strain, ε_o, where the strain rates are equal. Eqs. (A5) and (A6) yield:

$$\varepsilon_o = (\ln C_p - \ln C_t)/(D_t - D_p) \qquad \text{(A7)}$$

The minimum creep rate, $\dot{\varepsilon}_o$, is

$$\dot{\varepsilon}_o = C_p \cdot e^{D_p \cdot \varepsilon_o} = C_t \cdot e^{D_t \cdot \varepsilon_o} \qquad \text{(A8)}$$

Integration of Eq. (A5) yields

$$\varepsilon = -\frac{1}{D_p} \cdot \ln (1 - C_p \cdot D_p \cdot t), \qquad \text{(A9)}$$

which is the equation for the primary part of the creep curve.

Eqs. (A8) and (A9) give

$$t_o = -\frac{1}{C_p \cdot D_p} (e^{-D_p \cdot \varepsilon_o} - 1), \qquad \text{(A10)}$$

i.e. the primary - tertiary transition time.

Eqs. (A7) and (A10) show a very complicated, stress dependent relationship between ε_o and t_o. In practice, however, it was found that the rather complicated Eqs. (A7) and (A10) could be replaced by one of the following simple time dependent expressions for ε_o.

$$\varepsilon_o = E_1 + F_1 \cdot \log t \qquad \text{(A11a)}$$

$$\varepsilon_o = E_2 \cdot 10^{F_2 \cdot t} \qquad \text{(A11b)}$$

$$\varepsilon_o = E_3 / (1 + F_3/t) \qquad \text{(A11c)}$$

These expressions must be determined individually for the different structures since the relative amount of primary creep varies from structure to structure.

Finally, a mathematical expression for the tertiary creep stage can be derived from Eq. (A6).

$$\varepsilon = -\frac{1}{D_t} \cdot \left\{ \ln \left(e^{-D_t \cdot \varepsilon_o} - C_t \cdot D_t \cdot (t - t_o) \right) \right\} \qquad \text{(A12)}$$

ε_o and t_o are determined in Eqs. (A7) and (A10) respectively.

Contrary to many mathematical models for tertiary creep, Eq. (A12) yields a finite rupture time, t_R, i.e. the time for which ε in Eq. (A12) reaches infinity.

$$t_R = t_o + e^{-D_t \cdot \varepsilon_o} / (C_t \cdot D_t) \qquad (A13)$$

For comparison between experimental results and the results of the above-mentioned analysis regarding entire creep curves (Eqs. (A9) and (A12)), minimum creep rates (Eq. (A8)), or rupture times (Eq. (A13)), the reader is referred to the main report.

REFERENCES

A1 SAMUELSON, L.Å., Creep Buckling of Shells of Revolution. User's Manual for Program DSOR06. FFA Report HU 1548, Part 4, 1975.

A2 IVARSSON, B., and SANDSTRÖM, R., Creep Deformation and Rupture of Butt-Welded Tubes of Cold-Worked AISI 316 Steel. Metals Technology, 7, (1980), 440-48.

A3 IVARSSON, B., Creep of Butt-Welded AISI 316 (18Cr-13Ni-3Mo Steel) Tubes: Role of Plastic Strain and Primary Creep. Metals Technology, 9, (1982), 41-45

A4 SANDSTRÖM, R. and KONDYR, A., Model for Tertiary-Creep in Mo- and CrMo-Steels. In Proceedings of the Third International Conference on the Mechanical Behaviour of Materials (ICM3), Cambridge, England, 1979. 2 (1979), 275-84. Also in German: (Somewhat more extended) Kriechverformung, Anhäufung von Zeitstandsschädigungen und Voraussage der Restlebensdauer für drei Mo- und CrMo-Stähle. VGB-Kraftwerkstechnik 62, (1982), 802-13.

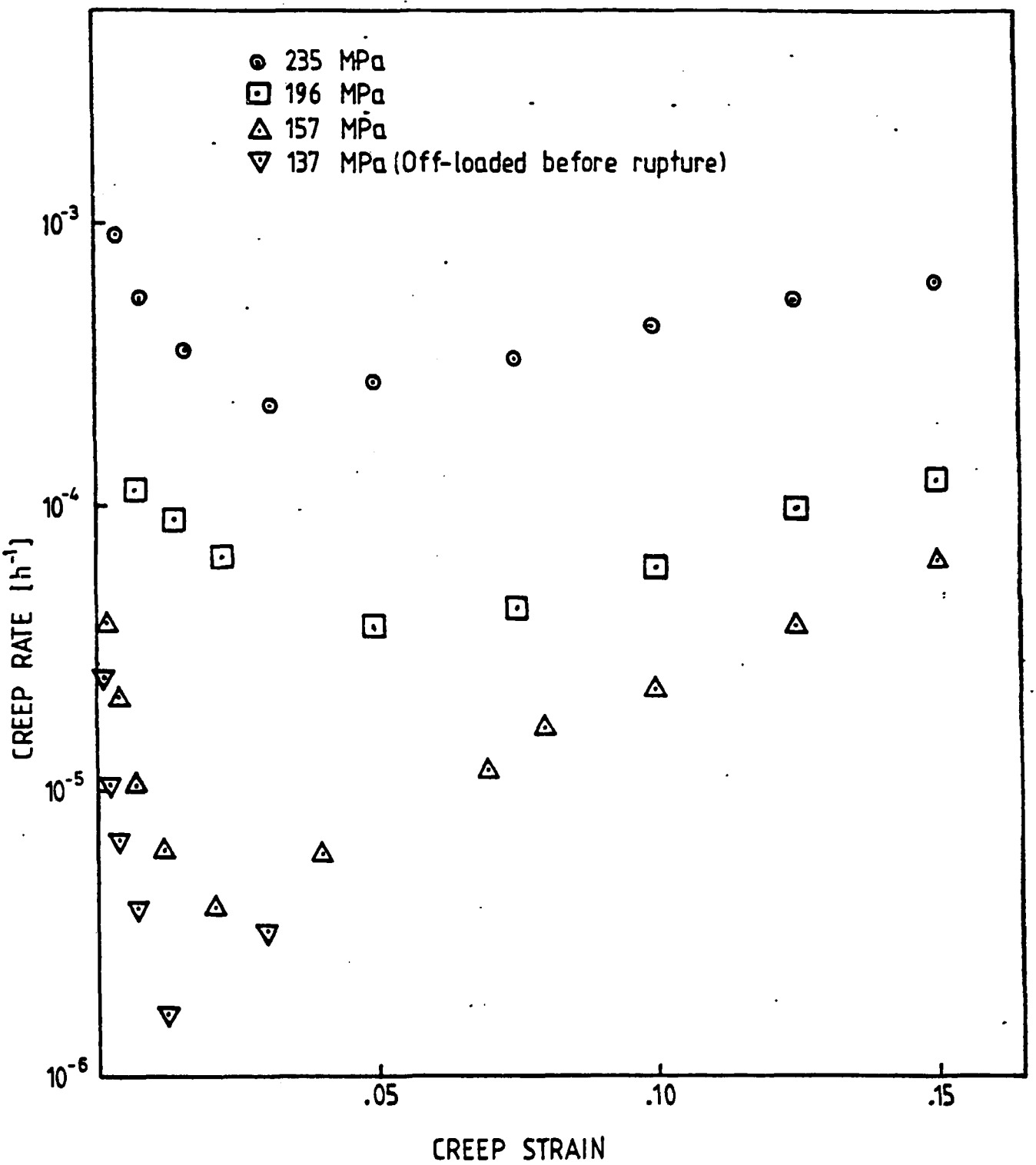

Fig. A1 Log (creep rate) against creep strain for an AISI 316 stainless steel tested at 600°C at four different stresses.

APPENDIX B. MODIFICATIONS OF THE CONSTITUTIVE EQUATIONS IN APPENDIX A

For some structures a different strain rate/strain relationship was valid than that used in Appendix A. Therefore some of the equations in Appendix A had to be changed. These equations are listed below with the same number as in Appendix A but with the A exchanged for an B.

$$\log \dot{\varepsilon} = a+b \cdot \log \varepsilon \tag{B2}$$

$$\log \dot{\varepsilon} = c+d \cdot \log \sigma + (e + f \cdot \log\sigma) \cdot \log \varepsilon \tag{B3}$$

$$\dot{\varepsilon} = 10^{(c+e \cdot \log\varepsilon)} \cdot \sigma^{(d+f \cdot \log\varepsilon)} \tag{B4}$$

$$\dot{\varepsilon}_p = C_p \cdot \varepsilon^{D_p} \tag{B5}$$

$$\dot{\varepsilon}_t = C_t \cdot \varepsilon^{D_t} \tag{B6}$$

$$C_p = 10^{(c+d \cdot \log\sigma)}$$

$$D_p = e + f \cdot \log\sigma$$

$$\varepsilon_o = (C_p/C_t)^{1/(D_t - D_p)} \tag{B7}$$

$$\dot{\varepsilon}_o = C_p \cdot \varepsilon_o^{D_p} = C_t \cdot \varepsilon_o^{D_t} \tag{B8}$$

$$\varepsilon = (C_p \cdot (1-D_p) \cdot t)^{1/(1-D_p)} \tag{B9}$$

$$t_o = \frac{\varepsilon_o^{(1-D_p)}}{C_p(1-D_p)} \qquad \text{(B10)}$$

$$\varepsilon = (\varepsilon_o^{(1-D_t)} + C_t(1-D_t)(t-t_o))^{1/(1-D_t)} \qquad \text{(B12)}$$

C_t is, although small, always positive. D_t is equivalent to b in Equation (B2) and hence positive for tertiary creep. Provided $D_t > 1$ a finite rupture time can be determined:

$$t_R = t_o - \varepsilon_o^{(1-D_t)} / C_t \cdot (1-D_t) \qquad \text{(B13)}$$

List of SKB reports

Annual Reports

1977–78
TR 121
KBS Technical Reports 1 – 120.
Summaries. Stockholm, May 1979.

1979
TR 79–28
The KBS Annual Report 1979.
KBS Technical Reports 79-01 – 79-27.
Summaries. Stockholm, March 1980.

1980
TR 80–26
The KBS Annual Report 1980.
KBS Technical Reports 80-01 – 80-25.
Summaries. Stockholm, March 1981.

1981
TR 81–17
The KBS Annual Report 1981.
KBS Technical Reports 81-01 – 81-16.
Summaries. Stockholm, April 1982.

1982
TR 82–28
The KBS Annual Report 1982.
KBS Technical Reports 82-01 – 82-27.
Summaries. Stockholm, July 1983.

1983
TR 83–77
The KBS Annual Report 1983.
KBS Technical Reports 83-01 – 83-76
Summaries. Stockholm, June 1984.

1984
TR 85–01
Annual Research and Development Report 1984
Including Summaries of Technical Reports Issued during 1984. (Technical Reports 84-01– 84-19)
Stockholm June 1985.

1985
TR 85-20
Annual Research and Development Report 1985
Including Summaries of Technical Reports Issued during 1985. (Technical Reports 85-01-85-19)
Stockholm May 1986.

1986
TR 86-31
SKB Annual Report 1986
Including Summaries of Technical Reports Issued during 1986
Stockholm, May 1987

1987
TR 87-33
SKB Annual Report 1987
Including Summaries of Technical Reports Issued during 1987
Stockholm, May 1988

Technical Reports

1988
TR 88-01
Preliminary investigations of deep ground water microbiology in Swedish granitic rocks
Karsten Pedersen
University of Göteborg
December 1987

TR 88-02
Migration of the fission products strontium, technetium, iodine, cesium and the actinides neptunium, plutonium, americium in granitic rock
Thomas Ittner[1], Börje Torstenfelt[1], Bert Allard[2]
[1]Chalmers University of Technology
[2]University of Linköping
January 1988

TR 88-03
Flow and solute transport in a single fracture. A two-dimensional statistical model
Luis Moreno[1], Yvonne Tsang[2], Chin Fu Tsang[2], Ivars Neretnieks[1]
[1]Royal Institute of Technology, Stockholm, Sweden
[2]Lawrence Berkeley Laboratory, Berkeley, CA, USA
January 1988

TR 88-04
Ion binding by humic and fulvic acids: A computational procedure based on functional site heterogeneity and the physical chemistry of polyelectrolyte solutions
J A Marinsky, M M Reddy, J Ephraim, A Mathuthu
US Geological Survey, Lakewood, CA, USA
Linköping University, Linköping
State University of New York at Buffalo, Buffalo, NY, USA
April 1987

TR 88-05
Description of geophysical data on the SKB database GEOTAB
Stefan Sehlstedt
Swedish Geological Co, Luleå
February 1988

TR 88-06
Description of geological data in SKBs database GEOTAB
Tomas Stark
Swedish Geological Co, Luleå
April 1988

TR 88-07
Tectonic studies in the Lansjärv region
Herbert Henkel
Swedish Geological Survey, Uppsala
October 1987

TR 88-08
Diffusion in the matrix of granitic rock. Field test in the Stripa mine. Final report.
Lars Birgersson, Ivars Neretnieks
Royal Institute of Technology, Stockholm
April 1988

TR 88-09
The kinetics of pitting corrosion of carbon steel. Progress report to June 1987
G P Marsh, K J Taylor, Z Sooi
Materials Development Division
Harwell Laboratory
February 1988

TR 88-10
GWHRT – A flow model for coupled groundwater and heat flow
Version 1.0
Roger Thunvik[1], Carol Braester[2]
[1] Royal Institute of Technology, Stockholm
[2] Israel Institute of Technology, Haifa
April 1988

TR 88-11
Groundwater numerical modelling of the Fjällveden study site – Evaluation of parameter variations
A hydrocoin study – Level 3, case 5A
Nils-Åke Larsson[1], Anders Markström[2]
[1] Swedish Geological Company, Uppsala
[2] Kemakta Consultants Co, Stockholm
October 1987

TR 88-12
Near-distance seismological monitoring of the Lansjärv neotectonic fault region
Rutger Wahlström, Sven-Olof Linder, Conny Holmqvist
Seismological Department, Uppsala University, Uppsala
May 1988

TR 88-13
Validation of the rock mechanics HNFEMP code against Colorado school of mines block test data
Ove Stephansson, Tomas Savilahti
University of Luleå, Luleå
May 1988

TR 88-14
Validation of MUDEC against Colorado school of mines block test data
Nick Barton, Panayiotis Chryssanthakis, Karstein Monsen
Norges Geotekniske Institutt, Oslo, Norge
April 1988

TR 88-15
Hydrothermal effects on montmorillonite. A preliminary study
Roland Pusch
Ola Karnland
June 1988

TR 88-16
Swedish Hard Rock Laboratory
First evaluation of preinvestigations 1986-87 and target area characterization
Gunnar Gustafson
Roy Stanfors
Peter Wikberg
June 1988

TR 88-17
On the corrosion of copper in pure water
T E Eriksen[1], P Ndalamba[1], I Grenthe[2]
[1] The Royal Institute of Technology, Stockholm
Department of nuclear chemistry
[2] The Royal Institute of Technology, Stockholm
Department of inorganic chemistry
March 1988

TR 88-18
Geochemical modelling of the evolution of a granite-concrete-water system around a repository for spent nuclear fuel
Bertrand Fritz, Benoit Madé, Yves Tardy
Université Louis Pasteur de Strasbourg
April 1988

TR 88-19
A Bayesian nonparametric estimation of distributions and quantiles
Kurt Pörn
Studsvik AB
November 1988

ISSN 0284-3757

CM-Tryck AB, Bromma 1988